Piezo1 mechanosensing regulates integrin-dependent chemotactic migration in human T cells

Chinky Shiu Chen Liu[1], Tithi Mandal[2], Parijat Biswas[3], Md. Asmaul Hoque[1,4], Purbita Bandopadhyay[1,4], Bishnu Prasad Sinha[1,4], Jafar Sarif[1,4], Ranit D'Rozario[1,4], Deepak Kumar Sinha[3], Bidisha Sinha[2], Dipyaman Ganguly[1]*

[1]IICB-Translational Research Unit of Excellence, CSIR-Indian Institute of Chemical Biology, Kolkata, India.

[2]Department of Biological Sciences, Indian Institute of Science Education and Research, Kolkata, India.

[3] Department of Biological Sciences, Indian Association for Cultivation of Science, Kolkata, India.

[4]Academy of Scientific and Innovative Research, Ghaziabad, India.

Correspondence: dipyaman@iicb.res.in

Running title: Piezo1 mechanosensing in human T cell chemotaxis

Keywords: Human T cells, Piezo1, Mechanosensing, Migration, Chemokine, Chemotaxis, Focal adhesion kinase, LFA-1, F-actin, Confocal Microscopy, Interference Reflection Microscopy

ABSTRACT

T cells are crucial for efficient antigen-specific immune responses and thus their migration within the body, to inflamed tissues from circulating blood or to secondary lymphoid organs, play a very critical role. T cell extravasation in inflamed tissues depends on chemotactic cues and interaction between endothelial adhesion molecules and cellular integrins. A migrating T cell is expected to sense diverse external and membrane-intrinsic mechano-physical cues, but molecular mechanisms of such mechanosensing in cell migration are not established. We explored if the professional mechanosensor Piezo1 play any role during integrin-dependent chemotaxis of human T cells. We found that deficiency of Piezo1 in human T cells interfered with integrin-dependent cellular motility on ICAM-1-coated surface. Piezo1 recruitment at the leading edge of moving T cells is dependent on and follows focal adhesion formation at the leading edge and local increase in membrane tension on chemokine receptor activation. Piezo1 recruitment and activation, followed by calcium influx and calpain activation, in turn are crucial for the integrin LFA-1 recruitment at the leading edge of the chemotactic human T cells. Thus we find that Piezo1 activation in response to local mechanical cues constitutes a membrane-intrinsic component of the 'outside-in' signaling in human T cells, migrating in response to chemokines, that mediates integrin recruitment to the leading edge.

INTRODUCTION

Efficient T cell migration from blood circulation to secondary lymphoid organs and inflamed tissue is paramount for optimal tissue antigen sampling and effector functions during adaptive immune response (1-4). The process is dependent on chemotactic cues, interaction between endothelial adhesion molecules and T cell integrins, and an intricate acto-myosin dynamics (5). Generation of mechanical force is critical to propel migrating cells (6-9). Mechanosensing of the substrate and increase in cellular membrane tension is also intuitively apparent in a migrating T cell, although mechanistic details are not explored to a great extent.

Piezo1 and Piezo2 ion channels are evolutionarily conserved professional mechanosensors that can sense increase in membrane tension mostly independent of other protein-protein interactions (10-12). Mechanosensing by Piezo1 has been demonstrated to play critical role in diverse patho-physiologic contexts given its wide tissue expression including the immunocellular compartment (13-21). We previously identified crucial role of this specialized mechanotransducer in optimal TCR triggering (14, 19). The immunocellular expression of Piezo1 thus makes it a strong candidate for mechanosensing at the plasma membrane to regulate motility of immune cells. Piezo1 shows differential involvement in cellular migration depending on context (22- 28). Previous studies point to the possibility of a role of Piezo1 in confinement sensing and integrin activation in moving cells, while it deters integrin-independent cell motility, usually referred to as amoeboid movement (29, 30).

Here we aimed at exploring if Piezo1 mechanosensing plays any role during integrin-dependent chemotactic migration of human T cell migration, a patho-physiologically critical event in an ongoing immune response as well as in the steady-state. We found that deficiency of Piezo1 expression in human $CD4^+$ T cells as well as Jurkat T cells interfered with efficient integrin-dependent cellular motility in response to a chemotactic cue. We also found that Piezo1 activation constitutes a hitherto unknown membrane-intrinsic component of the 'outside-in' signaling in human T cells in response to chemokine receptor activation, that follows activation of focal adhesion kinase leading to local increase in membrane tension and mediates local recruitment of integrin molecules at the leading edge of the moving human T cells.

RESULTS

Piezo1 deficiency abrogates integrin-dependent chemotactic motility in human T cells

We first assessed the role of Piezo1 on integrin-dependent, non-directional motility of primary human $CD4^+$ T cells. We used GFP plasmid and Piezo1 siRNA co-transfected cells to facilitate distinction between potentially transfected and untransfected cells during cell tracking. We compared the motility of GFP^+ T cells (presuming they had a good transfection efficiency and thus will also have the siRNA) with the GFP^- T cells in the same culture. This was confirmed by flow cytometric assessment of Piezo1 protein content on the T cell surface as well as the whole T cells (Supplemental figures 1B, C). Piezo1 deficiency in T cells (potentially GFP^+) significantly hindered their migration in response to CCL19 in terms of its mean-squared displacement (MSD, Figure 1A-C). Representative cell tracks of Piezo1 deficient (GFP^+) and control (GFP^-) are shown in Figure 1B and Supplementary Figure 1D.

ICAM1-coated transwell chemotaxis assay of human $CD4^+$ T lymphocytes and Jurkat T cells also showed significant reduction in migration upon siRNA-mediated Piezo1 knockdown, in response to CCL19 and SDF1α gradients, respectively (Figure. 1D, E). Piezo1 inhibition with GsMTx4 also led to significant impairment of transwell chemotaxis (Supplementary figure 1E).

Redistribution of Piezo1 toward the leading edge of migrating T cells in response to chemotactic cue

Cell polarity is a crucial aspect of directional cell motility in response to chemokines. $CD4^+$ T cells seeded on ICAM-1 bed showed striking polarity in Piezo1 distribution, upon stimulation with CCL19 for 15 minutes (Figure 1F, G; Supplemental video 1). Piezo1 m-Cherry expressing Jurkat T cells also showed striking leading edge polarity in the presence of SDF1α under ICAM1 adhesion (Figure 1H). In Figure 1I, particle image velocimetry (PIV) analysis of a single representative Jurkat cell has been shown to display the dynamically polarized Piezo1 fluorescence upon SDF1α treatment with time, as opposed to rather uniformly distributed Piezo1 signals in a representative untreated cell. The continuous redistribution of Piezo1 within the motile T cells towards the leading edge can also be appreciated in the representative moving image provided (Supplemental video 2).

Piezo1 redistribution in migrating T cells follow increased membrane tension in the leading edge

Piezo1 is a professional mechanosensor ion channel, which senses increase in plasma membrane tension and responds by driving calcium influx into the cells (14, 19, 31). As T cells migrate on substrate by extending membrane processes, it is intuitive to hypothesize that a component of

mechanosensing is incorporated in the mechanism of cellular movement. The data above, on a critical role of Piezo1 in migrating human T cells, also led us to hypothesize that Piezo1 mechanosensors may play a role in sensing mechanical cues in a moving T cell. So, first we aimed at confirming that there is polarized increase in tension in the leading edge plasma membrane of human T cells, moving in response to a chemotactic cue.

Cellular membrane tension can be measured by various techniques. However, most of the usual techniques, viz. atomic force microscopy or tension measurement using optical tweezers, are invasive and interfere with the membrane dynamics, as well as are difficult to employ on moving cells. We utilized the non-invasive technique of interference reflection microscopy or IRM for studying potential redistribution of membrane tension following chemokine stimulation (32, 33). In IRM technique, steady-state local fluctuations in the plasma membrane is imaged in cells adhered to a glass coverslip. The interference patterns generated due to continuously changing local distance between the coverslip and the plasma membrane are computed to derive the magnitude of local tension in the membrane – lower temporal fluctuations represent an increase in membrane tension (Figure. 2A). After baseline imaging, Piezo1-GFP expressing Jurkat cells were subjected to sequential fluorescence and IRM imaging post SDF1α addition which was followed over time. Chemokine administration to Jurkat T cells led to a decrease in temporal fluctuations and an increase in membrane tension when computed for the whole cellular contour (Figure 2B). The increase in membrane tension was registered within few minutes after chemokine addition and gradually declined over time (Figure 2C). Distribution of tension and fluctuation-amplitude in cells was also affected by the action of chemokine (Supplemental figure 2A) which was accompanied by increase in the membrane's degree of confinement and the effective viscosity experienced (Supplemental figure 2C & D). Moreover, the tension maps showed that the lamellipodial structures towards the leading edges of the cells had higher tension magnitudes (Figure 2D, Supplemental figure 2B). These high-tension edges are usually further emphasized at later time-points.

Finally, we explored if local membrane tension increase was linked to Piezo1 redistribution in the chemokine-experienced T cells. Of note here, during acquisition, there is typically a time delay of 1 minute between measurement of tension and Piezo1-GFP fluorescence. As expected, average tension peaked within the first few minutes of chemokine addition, followed by partial decline (Figure 2E) as seen for the whole cell. Pixel count of Piezo1-GFP intensity showed a similar pattern, albeit, at a delayed time, following the tension kinetics. In order to account for the delayed kinetics of tension magnitude and Piezo1-GFP pixel count, we performed a correlation between normalised Piezo1 pixel intensity at a particular time-frame, with normalised tension magnitude at the

131 preceding time frame. We observed significant positive correlation between the two parameters
132 (Figure 2F, G). Thus, IRM-coupled fluorescence microscopy revealed an increase in local membrane
133 tension in the leading edge of the moving T cells in response to chemokine receptor activation that
134 was associated with Piezo1 redistribution to the leading edges of the cells.

135

136 **Focal adhesion following chemokine receptor activation does not depend on Piezo1**

137 Focal adhesion formation is a critical step in cellular migration and activated (phosphorylated focal
138 adhesion kinases link extracellular physical cues to the cytoskeletal actomyosin scaffold (34, 35).
139 Chemokine signaling induces phosphorylation of focal adhesion kinase (FAK) and membrane
140 recruitment of the FAK complex forming focal adhesions with the extracellular substrate. FAK
141 recruits adapter proteins like paxillin to anchor with the local sub-membrane cytoskeleton made by
142 de novo F-actin polymerization. Membrane-recruited FAK complexes anchored to cytoskeleton
143 increases local membrane tension as well as recruit integrins to the membrane (36, 6, 37). This so-
144 called 'outside-in' signaling, whereby membrane recruitment of integrins (e.g.; LFA1 in T cells) is
145 initiated, is followed by integrin signaling ('inside-out' signaling) driven primarily by phosphoinositide
146 3-kinase (PI3K)-driven phosphorylation of Akt and downstream activation of Rho GTPases which in
147 turn drive extensive F-actin polymerization (38, 39). Retrograde flow of the F-actin to the rear end of
148 the moving cells, through myosin-based contractions, generates the propelling force for cells to
149 move forward following the chemokine gradient (6, 7).

150 Finding a critical role of Piezo1 in human T cell migration and a membrane tension-dependent
151 redistribution of Piezo1 to the leading edge of the moving cells led us explore if FAK recruitment to
152 the leading edge in response to chemokine stimulation was dependent on Piezo1. While
153 phosphorylated FAK (pFAK) showed striking polarity upon CCL19 stimulation on ICAM-1 beds (Figure
154 3A, B, Supplementary video 3), Piezo1 knockdown did not have any effect on pFAK polarity under
155 the same conditions (Figure 3C, D). Thus, focal adhesion formation following chemokine receptor
156 activation was not dependent on Piezo1. FAK activation recruits adapters like paxillin and vinculin
157 connecting the cortical cytoskeleton to the membrane and the extracellular matrix, thereby
158 increasing local membrane tension (34). Inhibition of FAK activation completely abrogated Piezo1
159 redistribution to the leading edge, hence the polarity (Figure 3E, F). This indicated that
160 mechanistically, FAK activation event precedes Piezo1 redistribution to the leading edge of the
161 migrating human $CD4^+$ T cells.

162

Membrane recruitment of LFA1 on chemokine receptor activation disrupts with Piezo1 deficiency

Integrin recruitment to the leading edge occurs downstream of FAK activation and local F-actin polymerization. As expected, CCL19 stimulation led to LFA1 recruitment to the leading edge upon CCL19 stimulation on ICAM1 bed (Figure 4A, B; Supplemental video 4). Moreover, Piezo1 and LFA1 exhibited significant colocalization upon chemokine stimulation (Figure 4C). Piezo1 downregulation abrogated LFA-1 polarity (Figure 4D, E; Supplemental videos 5, 6). Thus, role of Piezo1 in chemotactic migration of T cells was downstream of FAK assembly in response to chemokine receptor signaling, but preceded integrins recruitment. These data together point to a mechanism whereby local increase in membrane tension leading from FAK activation and assembly drives Piezo1 activation, which in turn is linked to LFA1 recruitment to the focal adhesions.

To further confirm this critical role of Piezo1 on LFA1 recruitment, we looked at the major signaling event downstream of LFA1 recruitment to the leading edge, i.e., phosphorylation of Akt downstream of PI3K activation, which in turn is triggered upon integrin activation. On treatment with CCL19, human $CD4^+$ T cells moving on ICAM-1-coated plates did show a prominent leading-edge polarity of non-phosphorylated and phosphorylated Akt (pAkt) (Figure 4F, control panel). But in Piezo1-deficient cells the polarity of pAkt is abrogated (Figure 4G), not affecting the polarity of non-phosphorylated AKT (Figure 4H; Supplemental videos 7, 8), substantiating the cellular signaling defect due to non-recruitment of LFA1 to the leading edge membrane.

Piezo1 deficiency disrupts F-actin retrograde flow in T cells despite chemokine receptor activation

Piezo1-mediated sensing of membrane tension drives calcium ion influx, which in turn has been shown to activate calpain and F-actin polymerization (14, 19). LFA1 recruitment is driven by local actin scaffold formation following FAK assembly, which as our data indicates is perhaps contributed by consolidation local actin scaffold downstream of Piezo1 activation. To confirm this, we performed Ca^{2+} imaging in Piezo1-mCherry transfected Jurkat Cells using total internal reflection fluorescence (TIRF) microscope in response to chemokine. We found significant colocalization of the Ca^{2+} signal with the Piezo1 signal on the chemokine treated Jurkat cells (Figure 5A, B; Supplemental figure 3A, B). Next to confirm that activation of calpain mediates the Piezo1 function, we observed that prior inhibition with calpain inhibitor PD150606 abrogated CCL19-induced LFA1 recruitment to the leading edge of the T cells (Figure 5C, D). As expected, the upstream event of pFAK polarity was not affected by the calpain inhibition (Supplemental figure 3C, D).

While F-actin polymerization downstream of FAK is required for LFA1 recruitment, LFA1 in turn drives a more robust F-actin polymerization at the leading edge, through Akt/Rho GTPase activation.

Leading edge F-actin undergoes retrograde flow due to myosin contractions, thereby enabling cells to move forward. Thus, both at the leading edge lamellipodia and the rear edge F-actin redistribution can be documented in a motile cell. We observed focal co-localization of LFA1 with F-actin at the leading edge, along with a denser actin-rich protrusion in the rear edge or the uropod (Figure 5C), which was abolished upon calpain inhibition (Figure 5C, E). Hence, LFA1 recruitment may depend on local F-actin polarization downstream of Piezo1 activation. On the other hand, failure of LFA1 recruitment and activation halts further F-actin polarization feeding the retrograde flow of actin during migration.

Dichotomy of Piezo1 (dense leading edge distribution) and F-actin (more dense at the rear end) distribution was clearly demonstrated in cells stimulated with chemokine (Figure 6A and Supplemental video 9). But, no F-actin polarity was seen on downregulating Piezo1 in the T cells (Figure 6B, C; Supplemental videos 10, 11). Live cell imaging of Jurkat T cells expressing Piezo1-mCherry and actin-GFP on ICAM-1 coated dishes was performed in the presence or absence of SDF1α (Supplemental figure 4A). Chemokine addition showed significant increase in Piezo1 polarity to the front end, as shown in the earlier experiments (Figure 6E, Supplemental figure 4B, left) upon chemokine stimulation when compared to untreated cells (Figure 6D, Supplemental figure 4B, left). But F-actin showed a dynamic balance at both ends as expected (Figure 6E, Supplemental figure 4F, right). Polar plots depicting angular distribution of Piezo1 mCherry and actin-GFP (over all time-points) in the presence or absence of SDF1α are shown in Supplemental figure 4C. Representative image 6F and supplemental video 12 shows Piezo1-mCherry distribution predominantly at the leading edge and actin-GFP eventually accumulating at the rear end in uropod-like cellular extensions in a migrating Jurkat T cell.

Thus, our data reveals a membrane-intrinsic event, involving a critical role of Piezo1 mechanosensors, within the outside-in signaling module in response to chemokine receptor activation in human T cells. The mechanistic model derived from our data is depicted in Figure 7. The Piezo1 mechanosensing links the focal adhesion assembly to integrins recruitment at the leading edge of the human T cells migrating in response to chemokine activation and thus play a critical role in chemotactic migration of human T cells.

DISCUSSION

The present study explored the role of membrane-intrinsic tension generation and the crucial role of sensing this physical cue in the context of human T cell migration in response to chemokine receptor

activation. Deficiency of Piezo1 inhibited integrin-dependent migration, demonstrating crucial role of these mechanosensors in this mode of T cell migration. As the integrin-dependent chemotactic migration of T cells is a critically implicated in most patho-physiologic contexts, in the present study we focused on the potential role of Piezo1 mechanosensors in this specific context.

Notably, a previous study in vivo in mice, using genetic deletion of Piezo1 in T cells, reported no significant effect on tissue recruitment of T cells (17). Although a functional redundancy in the role of Piezo1-mediated mechanosensing in mouse T cells warrants exclusion, especially in case of gene deletion in developing T cells, given the considerable expression of Piezo2 as well in mouse T cells (40). On the other hand, a role of Piezo1 activation in fibroblastic reticular cells in Peyer's patches has been shown to regulate lymphocyte migration through tissue conduits (41). The different tissue distribution of Piezo1 and Piezo2 expression in humans warranted exploring the role of Piezo1 in migrating human T cells, as in humans Piezo2 is hardly expressed in the hematopoietic cells.

Non-invasive interference reflection microscopy allowed us to demonstrate dynamic change in membrane tension at the leading edge of T cells stimulated with chemokine on ICAM1-bed which was closely followed by dynamic recruitment Piezo1 locally. Chemokine receptor activation leads to focal adhesion formation at the leading edge of the migrating T cells (34, 35). Our experiments revealed that Piezo1 recruitment at the leading edge of the cells followed focal adhesion kinase activation. Focal adhesions do increase local membrane tension as they connect the extracellular environment with the cortical cytoskeleton of the cell (34). Piezo1 recruitment locally seems to be a response to this membrane tension increase at focal adhesions.

'Outside-in' signaling downstream of focal adhesion formation recruits integrins to the leading edge of the moving T cells (35, 36) which was abrogated by Piezo1 downregulation. Piezo1 has been shown to drive Ca^{2+} influx into the T cells leading to calpain activation (14, 19). As expected, calpain inhibition also interfered with leading edge recruitment of the integrin LFA-1. Plausibly calpain activation drives local F-actin polymerization at the leading edge facilitating LFA-1 recruitment. This was also supported by loss of polarity of AKT phosphorylation with Piezo1 deficiency, which is known to be the major downstream signaling module that succeeds LFA-1 recruitment and activation (39, 42). These dysregulations in turn abrogates the retrograde flow of actin in the moving cell that is essential for forward propulsion of the cell body (6, 7, 37, 41). Of note here, a role of ER-resident Piezo1, in driving R-RAS-driven activation of integrins, which was again dependent on calpain activation, was reported even before the mechanosensing function of Piezo1 was established (30).

Thus, the present study reports a hitherto unexplored role of the professional mechanosensor Piezo1 in integrin dependent chemotactic movement of human T cells. In the cascade of leading edge events in a moving human T cell, following chemokine receptor activation and eventually leading to the retrograde flow of actin, focal adhesion formation precedes Piezo1 activation, while LFA-1 recruitment is dependent on Piezo1 function.

METHODS

Human $CD4^+$ T cell isolation and transfection.

Human $CD4^+$ T lymphocytes were isolated from peripheral blood from healthy donors through magnetic immunoselection. Peripheral blood samples from healthy human subjects were collected on obtaining written informed consents. The studies were approved by the Human Ethics Committee of CSIR-Indian Institute of Chemical Biology, India. Cells were transfected with either EGFP control or Piezo1-specific siRNAs using Lonza 4D nucleofector, as per the manufacturer's protocol. Briefly, cells were nucleofected in 100µl of supplemented P3 primary buffer containing 175ng of respective siRNAs. Nucleofection was performed using EO-115 pulse in Lonza 4D nucleofector. Nucleofected cells were incubated at 37°C. 5% CO_2 in RPMI media containing 10% FBS for 3 days before experiments were conducted. Knockdown was checked by qPCR measurement of Piezo1 and Piezo2 transcript levels (Supplementary Figure. 1A).

GFP/Piezo1 siRNA co-nucleofection

Approximately 2×10^6 human CD4+ T lymphocytes were nucleofected with 3µg of GFP-expressing plasmid along with 175ng of Piezo1-specific siRNA. Cells were incubated for 3 days before migration studies.

Analysis of Piezo1 knockdown

GFP and Piezo1 siRNA co-transfected $CD4^+$ T cells were stained for Piezo1 to measure downregulation. Both surface and intracellular (0.2% triton X-100 permeabilization) Piezo1 were stained. Briefly, cells were collected on day and fixed in 0.5% PFA for 5 minutes on ice. Cells were stained with 1.67µg/ml of rabbit anti-Piezo1 for 45 minutes at 4°C. After washing, 1.5µg/ml of anti-rabbit alexa 568-IgG was added and incubated for 30 minutes at 4°C. Cells were acquired on BD LSR Fortessa III after washing. Piezo1 mean fluorescence intensity (MFI) were measured both for GFP^+ and GFP^- cells.

2-dimensional cell tracking.

12-mm confocal dishes were coated with 4µg/ml of recombinant human ICAM-1 overnight at 4°C. Wells were washed with 1X PBS. Tracking of GFP/Piezo1 siRNA-transfected cells were performed after cell trace violet-labelling in the presence of recombinant CCL19 on ICAM1-coated dishes. Stained cells were added to the wells and allowed to settle for 1 hour at 37°C. 2D tracking was performed at 37°C after addition of 0.5µg/ml of recombinant human CCL19 and incubated for 10 minutes before acquisition. Images were acquired at regular intervals at room temperature using Zeiss LSM setup at 20X magnification for a total duration of 10-15 minutes at 30 second interval. $CD4^+$ T lymphocytes were RPMI without phenol red supplemented with 10% FBS and 25mM HEPES during the duration of imaging.

2D cell tracking analysis

For tracking analyses of GFP and Piezo1 siRNA co-transfected cells, all cells above a specific threshold area were used to eliminate potential debris and dead cells due to GFP plasmid transfection. Time-based image stacks obtained were analysed using the Particle Tracker 2D/3D plugin of the FIJI Mosaic Suite. Briefly, images were corrected for any shift in alignment during acquisition, using the StackReg plugin. Corrected images were the thresholded to create a 0-255 binary mask which were then used for tracking using the Particle Tracker 2D/3D plugin. Tracking provided frame-wise X-Y co-ordinates of cells which were subsequently used to derive the following parameter to measure motility:

a. Mean-squared displacement

$MSD\ (n) = \sum_{i=0}^{i=n}(x_n - x_0)^2 + (y_n - y_0)^2$ where,

i = 0 is the first frame,

i = n is the n^{th} frame.

Tranwell chemotaxis assay

5µm transwell inserts were coated with 4µg/ml of recombinant human ICAM-1. Equal number of primary human $CD4^+$ T cells and Jurkat cells nucleofected with control or Piezo1-specific siRNA were added to the ICAM-1-coated inserts. Cells were allowed to migrate in response to recombinant human CCL19 (0.5µg/ml) or SDF1α (0.1µg/ml) in the lower chamber wells for 5 hours and 1.5 hours, respectively, at 37°C, 5% CO_2. Migration was halted by placing the setup on ice. Percent migration

was calculated by counting the number of cells in the lower chamber and dividing it by total number of cells that was seeded.

Overexpression of mCherry/GFP-tagged Piezo1 and Actin-GFP in Jurkat cells.

GFP and mCherry-tagged Piezo1 constructs were kindly provided by Dr. Charles Cox at Victor Chang Cardiac Research Laboratory, Darlinghurst, Australia. Approximately 2 million Jurkat cells were nucleofected with 2-3µg of fluorescent Piezo1 construct in 100µl of supplemented SE cell line buffer. Cells were pulsed using CL-120 program in Lonza 4D nucleofector. Cells were cultured in antibiotics-deficient RPMI supplemented with 20% FBS for 36 hours. Overexpression was confirmed using flow cytometry.

Interference Reflection Microscopy and Analysis

Jurkat cells were nucleofected with 2-3µg/ml of Piezo1-GFP construct. Overexpression was confirmed using flow cytometry. Transfected cells were seeded on recombinant human fibronectin glass-based dishes. Cells were allowed to completely adhere for 1 hour to allow IRM imaging.

An inverted microscope (Nikon, Japan) with 60x 1.2 NA water-immersion objective, Hg arc lamp and necessary interference filter (546 ± 12 nm) were used for the interference reflection microscopy (43, 44) and images were captured at 19.91 frames per second using a EMCCD camera (Evolve 512 Delta; Photometrics, Trenton, NJ). Cells that were significantly adhered to the glass bottom were used for imaging. Regions used for analysis were stringently chosen to avoid parts farther than ~ 100 nm from the coverslip – also called the first branch region (FBR) and the size chosen was 4x4 pixels corresponding to ~ $(720\ nm)^2$. First, cells were imaged by IRM to take baseline reading following which chemokine (SDF1α) was added. Cells were followed till 30 min with ~ 2-3 min interval post-chemokine addition.

For stringent selection of subset of regions, extraction of parameters as well as for visualizing the amplitude of fluctuations, the methodology developed previously (44, 45) was followed. 2048 frames corresponding to ~ 102 sec were captured and used for a single measurement of tension. The analysis involved calculation of standard deviation of temporal height fluctuations (SD_{time}) and estimating the power spectral density (PSD) by autoregressive technique (probability of covariance or pcov) where the order is chosen to match best with PSD obtained using fast fourier transform (MATLAB, Mathworks Inc., USA). For deriving mechanical parameters, the PSD is fitted with a Helfrich-based model –

$$PSD(f) = \frac{4\eta_{eff} A k_B T}{\pi} \int_{q_{min}}^{q_{max}} \frac{dq}{(4\eta_{eff}(2\pi f))^2 + \left[\kappa q^3 + \sigma q + \frac{\gamma}{q}\right]^2}$$

with four fitting parameters (44) using fluctuation-tension (σ), effective viscosity (η_{eff}), level of confinement (γ) and the effective active temperature (A)). The bending rigidity (κ) was fixed at 15 k_BT. Membrane fluctuation-tension closely follows membrane frame tension for a large range of tension values (46). Membrane fluctuation-tension closely follows membrane frame tension for a large range of tension values (46). For brevity, membrane fluctuation-tension has been referred to as "tension" in the rest of the manuscript. Tension maps were created from PSDs calculated for every pixel which were subsequently fitted and parameters extracted for every pixel. For analysing correlation between fluorescence and tension, first the fluorescence distribution of cells was plotted. Regions of intermediate intensity (around the first peak of the distribution) of a fixed intensity range was filtered and the pixel count of the filtered area was plotted against the average tension in those pixels. Normalization was done by diving by the maximum value in the time series. Normalized pixel count, thus, reflects how area with high Piezo1-GFP at the membrane changes while avoiding a small area fraction with very high Piezo1-GFP which might arise from internal structures. To ensure significance of the observed differences, the statistical test undertaken was the Mann-Whitney U test.

Piezo1 and actin distribution in live cell imaging

Jurkat cells expressing mCherry-tagged Piezo1 were seeded on ICAM-1-coated dishes. 0.1µg/ml of recombinant human SDF1α was added to the cells for 15 minutes prior to imaging. Cell tracking was performed in EVOS FL microscope using the PE-Texas red filter, at an interval of 1 frame per minute, at room temperature. Imaging was performed for a total duration of 15 minutes.

For Jurkat cells transfected with Piezo1-mcherry and actin-GFP, cells were treated similarly and acquired on Zeiss LSM confocal setup. Z-stack was obtained at 1µm per stack to capture the entire cell. Time-lapse was imaged at an interval of 30 second per frame for a total duration of 5 minutes. Confocal imaging was performed at 37°C.

For particle image velocimetry (PIV) analysis of Piezo1-mCherry-expressing Jurkat cells was performed using the Iterative PIV plugin of FIJI. Time-lapse image stacks were split and stacks of paired subsequent images were formed. Each of these stacks was then corrected for any shift in alignment using the StackReg plugin. Aligned stacks were then subjected to iterative FIJI PIV analysis using the conventional cross-correlation method to measure flow of fluorescent Piezo1 in

chemokine-treated Jurkat cells. PIV post-processing was done with default parameters and PIV magnitude plots were obtained from the plugin.

Measurement of cell polarity during live-cell imaging.

A custom code was written in Fiji (ImageJ) to analyze the cell image time-lapse for the calculation Front/Back (F/B) ratio of actin and Piezo1 expression relative to the direction of cell migration. Briefly, intensity-based thresholding was performed on the actin images to create binary masks of the cells. Individual cell boundaries were identified in the time-lapse, which were stored in the form of polygon ROIs. The cell ROIs enabled the computation of each cell's trajectory and displacement vectors from the geometrical centroid at every frame of the time-lapse video. The computation of cell polarity involved fitting each cell's ROI to an ellipse and bisecting the ellipse perpendicular to the migration direction. The ratio of total intensities in the leading half and the trailing half of the ellipse was calculated for actin and piezo1 images to get the F/B ratio.

For polarity measurement of fixed confocal images, cell boundaries were similarly identified. Stored ROIs were then split into two halves perpendicular to the long axis of the cell. The polarity index was measured by calculating the difference of total intensities of two halves of the cell divided by the sum of their total intensities. A measurement of 1 shows complete skewing of fluorescent signals to one half of the cell, while a value of 0 shows uniform distribution of fluorescent signals in both cell halves Representative polarity analysis Piezo1 (fixed), Piezo1 mCherry (live), pFAK (fixed), CD11a/LFA-1 (fixed) and actin (fixed) of untreated and CCL19-stimulated $CD4^+$ T lymphocytes (Supplemental figure 6A-F).

Generation of Piezo1 mCherry and Actin-GFP polar plots.

For analysis of angular/spatial distribution of Piezo1 mCherry and actin-GFP with respect to direction of cell movement, cell ROIs were applied to the actin and piezo1 channels individually, to find the intensity-weighted centre of mass (through all the time-points). Depending on the fluorescence intensity distribution, the intensity-weighted centre of mass is shifted away from the geometric centroid and towards the direction of a higher protein distribution. Thus, a vector connecting the centroid (geometric centre) to the centre of mass gives the direction of polarization of the protein of interest. The relative angle of the polarization vector against the cell displacement vector was calculated for each frame, and a polar histogram of the angles was plotted for actin-GFP and piezo1-mCherry.

Fixed immunostaining for confocal imaging

Untransfected human $CD4^+$ T lymphocytes were seeded on 12-mm, ICAM-1-coated glass coverslips at a density of about 0.2 million cells per coverslip. Cells were incubated at 37°C, 5% CO_2 for 1.5 hours. 0.5µg/ml of recombinant human CCL19 was added to each coverslip and incubated for 20-30 minutes at 37°C. Post-treatment, cells were fixed in 4% paraformaldehyde for 15 minutes at room temperature. Blocking was performed in 3% bovine serum albumin in 1X PBS containing 0.2% Triton X-100 for 50 minutes at room temperature. Primary rabbit anti-human Piezo1 (Proteintech) was added at a dilution of 1:100 (5µg/ml) and incubated at room temperature for 1 to 1.5 hours. Alexa 568-conjugated anti-rabbit IgG was added at a dilution of 1:350 (5.7µg/ml), and incubated for further 45-50 minutes. Nuclear staining was performed for 1 minute with Hoechst 33342 dye at a concentration of 1µg/ml in 1X PBS. All washes between steps were carried out in 1X PBS. Stained cells were then mounted on Vectashield® mounting media and sealed before confocal imaging. For Piezo1 and CD44 co-staining, rabbit anti-Piezo1 and mouse anti-human CD44 were used at a concentration of 5µg/ml, each. Alexa 488-conjugated anti-rabbit IgG and alexa 633-conjugated anti-mouse IgG were used at a concentration of 5.7µg/ml, each.

For actin imaging, LifeAct-TagGFP2 protein was added at a concentration of 0.5µg/ml, and incubated for 45 minutes at room temperature before washing. For LFA-1 ($\alpha_L\beta2$) staining, mouse anti-human CD11a (α_L subunit) was added at a concentration of 5µg/ml, followed by addition of anti-mouse Alexa 594-conjugated IgG. For LFA-1 and Piezo1 co-staining, primary antibodies were added at above concentrations, with Alexa 568-conjugated anti-rabbit IgG (for Piezo1) and Alexa 488-conjuagted anti-mouse IgG (for CD11a/LFA-1). Rabbit/mouse anti-phosphorylated FAK (Tyr-397) was used to stain pFAK to detect focal adhesions. These cells were treated with chemokine CCL19 for 10 minutes prior to fixation. While doing confocal microscopy, Z-stacks were captured at 0.5µm intervals. Confocal images are represented are maximum intensity projections of the Z-slices. 3Dprojectionfunction of Fiji was used to create a 3D rendering of the Z-slices, using the brightest point method of projection.

TIRF Imaging and Ca^{2+}-Piezo1 colocalization

Ca^{2+}-Piezo1 imaging involved incubating cells with Fluo-3 AM (2.5 µM) in HBSS buffer for 30 minutes at 37˚C, followed by washing and imaging in RPMI containing 10% FBS, and 25 mM HEPES media. Jurkat cell were transfected with Piezo1 mCherry plasmid and only those expressing Piezo1 mCherry were selected for the study. Dual-colour sequential TIRF imaging was employed, with Piezo1 mCherry being imaged at 300 ms (100 frames) and Ca2+ imaging performed using a 10 ms exposure time (2000 frames). The short exposure for Ca2+ was used to capture transient local peaks of fluorescence which would otherwise average out at longer exposure times. The maximum projection

of the time series was used to detect local peaks using adaptive local thresholding (MATLAB), and a size filter was used to exclude large objects identified with a relatively low Ca^{2+} gradient. For each specific set of settings, the Ca^{2+} signal objects detected were used to calculate the average cluster size and total area of objects. Uniform random numbers were used to simulate clusters with appropriate probability to ensure that the final area of the simulated Ca^{2+} clusters closely matched the real data. The overlap between the real Ca^{2+} signal and Piezo1 objects was compared with the simulated data to test for deviation from a random placement of Ca^{2+} spots. To assess the robustness of the results, different combinations of size filters of Piezo1 and Ca^{2+} objects were used, ranging from 50 to 350 pixels.

Calpain Inhibition

PD150606 (Merck, India), a non-competitive calpain 1 and 2 inhibitors, was used at a concentration of 100µM. Untransfected $CD4^+$ T lymphocytes were treated with PD150606 for 1 hour at 37°C prior to treatment of chemokine. Post -chemokine treatment cells were stained either with pFAK as described.

Focal adhesion kinase Inhibition

FAK inhibitor 14 (1,2,4,5-Benzenetetraamine tetrahydrochloride) was used to selectively inhibit FAK activity. Inhibitor was added at a final concentration 10µM, 1 hour prior to treatment with recombinant CCL19. Post-treatment with CCL19, $CD4^+$ T lymphocytes were stained with Piezo1 for confocal imaging.

Piezo1 Inhibition

Primary human $CD4^+$ T cells were incubated with 10µM of GsMTx4 for 1 hour prior to transwell chemotaxis assay in response to recombinant CCL19.

Statistics

Student t-test was used to calculate significance.

ACKNOWLEDGEMENTS

The study was funded by Council of Scientific and Industrial Research, India (Grant no. FBR MLP-140). D.G. is a recipient of Swarnajayanti Fellowship from Department of Science and Technology,

Government of India. The authors express their gratitude for provision of the Piezo1 constructs by Dr. Charles Cox, Victor Chang Institute of Cardiac Research, Australia.

The authors declare no competing interests

C.S.C.L. designed, performed and analyzed most of the experiments, prepared the figures and took part in writing the manuscript; T.M., B.S. and C.S.C.L. performed the IRM experiments; T.M. and B.S. analyzed IRM data; C.S.C.L., P.B. and D.K.S. performed image analyses; Pu.B., M.A.H., B.P.S., J.S. and R.D. helped with cell culture and confocal microscopy experiments; D.G. conceptualized and supervised the study, acquired funding, designed experiments and wrote the manuscript with input from all authors.

REFERENCES

1. Shechter R, London A, Schwartz M. Orchestrated leukocyte recruitment to immune-privileged sites: absolute barriers versus educational gates. Nat Rev Immunol. 2013 Mar;13(3):206-18. doi: 10.1038/nri3391.
2. Krummel MF, Bartumeus F, Gérard A. T cell migration, search strategies and mechanisms. Nat Rev Immunol. 2016 Mar;16(3):193-201. doi: 10.1038/nri.2015.16.
3. Woodland DL, Kohlmeier JE. Migration, maintenance and recall of memory T cells in peripheral tissues. Nat Rev Immunol. 2009 Mar;9(3):153-61. doi: 10.1038/nri2496.
4. Masopust D, Schenkel JM. The integration of T cell migration, differentiation and function. Nat Rev Immunol. 2013 May;13(5):309-20. doi: 10.1038/nri3442.
5. Fowell DJ, Kim M. The spatio-temporal control of effector T cell migration. Nat Rev Immunol. 2021 Sep;21(9):582-596. doi: 10.1038/s41577-021-00507-0.
6. Dupré L, Houmadi R, Tang C, Rey-Barroso J. T Lymphocyte Migration: An Action Movie Starring the Actin and Associated Actors. Front Immunol. 2015 Nov 18;6:586. doi: 10.3389/fimmu.2015.00586.
7. Nordenfelt P, Moore TI, Mehta SB, Kalappurakkal JM, Swaminathan V, Koga N, Lambert TJ, Baker D, Waters JC, Oldenbourg R, Tani T, Mayor S, Waterman CM, Springer TA. Direction of actin flow dictates integrin LFA-1 orientation during leukocyte migration. Nat Commun. 2017 Dec 11;8(1):2047. doi: 10.1038/s41467-017-01848-y.
8. Moreau HD, Piel M, Voituriez R, Lennon-Duménil AM. Integrating Physical and Molecular Insights on Immune Cell Migration. Trends Immunol. 2018 Aug;39(8):632-643. doi: 10.1016/j.it.2018.04.007.

9. Shannon MJ, Pineau J, Griffié J, Aaron J, Peel T, Williamson DJ, Zamoyska R, Cope AP, Cornish GH, Owen DM. Differential nanoscale organisation of LFA-1 modulates T-cell migration. J Cell Sci. 2019 Oct 16;133(5):jcs232991. doi: 10.1242/jcs.232991.
10. Coste B, Mathur J, Schmidt M, Earley TJ, Ranade S, Petrus MJ, Dubin AE, Patapoutian A. Piezo1 and Piezo2 are essential components of distinct mechanically activated cation channels. Science. 2010 Oct 1;330(6000):55-60. doi: 10.1126/science.1193270.
11. Coste B, Xiao B, Santos JS, Syeda R, Grandl J, Spencer KS, Kim SE, Schmidt M, Mathur J, Dubin AE, Montal M, Patapoutian A. Piezo proteins are pore-forming subunits of mechanically activated channels. Nature. 2012 Feb 19;483(7388):176-81. doi: 10.1038/nature10812.
12. Syeda R, Florendo MN, Cox CD, Kefauver JM, Santos JS, Martinac B, Patapoutian A. Piezo1 Channels Are Inherently Mechanosensitive. Cell Rep. 2016 Nov 8;17(7):1739-1746. doi: 10.1016/j.celrep.2016.10.033.
13. Murthy SE, Dubin AE, Patapoutian A. Piezos thrive under pressure: mechanically activated ion channels in health and disease. Nat Rev Mol Cell Biol. 2017 Dec;18(12):771-783. doi: 10.1038/nrm.2017.92. Epub 2017 Oct 4. PMID: 28974772.
14. Liu CSC, Raychaudhuri D, Paul B, Chakrabarty Y, Ghosh AR, Rahaman O, Talukdar A, Ganguly D. Cutting Edge: Piezo1 Mechanosensors Optimize Human T Cell Activation. J Immunol. 2018 Feb 15;200(4):1255-1260. doi: 10.4049/jimmunol.1701118.
15. Atcha H, Jairaman A, Holt JR, Meli VS, Nagalla RR, Veerasubramanian PK, Brumm KT, Lim HE, Othy S, Cahalan MD, Pathak MM, Liu WF. Mechanically activated ion channel Piezo1 modulates macrophage polarization and stiffness sensing. Nat Commun. 2021 May 31;12(1):3256. doi: 10.1038/s41467-021-23482-5.
16. Geng J, Shi Y, Zhang J, Yang B, Wang P, Yuan W, Zhao H, Li J, Qin F, Hong L, Xie C, Deng X, Sun Y, Wu C, Chen L, Zhou D. TLR4 signalling via Piezo1 engages and enhances the macrophage mediated host response during bacterial infection. Nat Commun. 2021 Jun 10;12(1):3519. doi: 10.1038/s41467-021-23683-y.
17. Jairaman A, Othy S, Dynes JL, Yeromin AV, Zavala A, Greenberg ML, Nourse JL, Holt JR, Cahalan SM, Marangoni F, Parker I, Pathak MM, Cahalan MD. Piezo1 channels restrain regulatory T cells but are dispensable for effector CD4+ T cell responses. Sci Adv. 2021 Jul 7;7(28):eabg5859. doi: 10.1126/sciadv.abg5859.
18. Jäntti H, Sitnikova V, Ishchenko Y, Shakirzyanova A, Giudice L, Ugidos IF, Gómez-Budia M, Korvenlaita N, Ohtonen S, Belaya I, Fazaludeen F, Mikhailov N, Gotkiewicz M, Ketola K, Lehtonen Š, Koistinaho J, Kanninen KM, Hernández D, Pébay A, Giugno R, Korhonen P,

533 Giniatullin R, Malm T. Microglial amyloid beta clearance is driven by PIEZO1 channels. J
534 Neuroinflammation. 2022 Jun 15;19(1):147. doi: 10.1186/s12974-022-02486-y.
535 19. Liu CSC, Ganguly D. Mechanical Cues for T Cell Activation: Role of Piezo1 Mechanosensors.
536 Crit Rev Immunol. 2019;39(1):15-38. doi: 10.1615/CritRevImmunol.2019029595.
537 20. Ma S, Dubin AE, Zhang Y, Mousavi SAR, Wang Y, Coombs AM, Loud M, Andolfo I,
538 Patapoutian A. A role of PIEZO1 in iron metabolism in mice and humans. Cell. 2021 Feb
539 18;184(4):969-982.e13. doi: 10.1016/j.cell.2021.01.024.
540 21. He Y, Deng B, Liu S, Luo S, Ning Y, Pan X, Wan R, Chen Y, Zhang Z, Jiang J, Xu H, Xia M, Li J.
541 Myeloid Piezo1 Deletion Protects Renal Fibrosis by Restraining Macrophage Infiltration and
542 Activation. Hypertension. 2022 May;79(5):918-931. doi:
543 10.1161/HYPERTENSIONAHA.121.18750.
544 22. Huang Z, Sun Z, Zhang X, Niu K, Wang Y, Zheng J, Li H, Liu Y. Loss of stretch-activated
545 channels, PIEZOs, accelerates non-small cell lung cancer progression and cell migration.
546 Biosci Rep. 2019 Mar 22;39(3): BSR20181679. doi: 10.1042/BSR20181679.
547 23. Chubinskiy-Nadezhdin VI, Vasileva VY, Vassilieva IO, Sudarikova AV, Morachevskaya EA,
548 Negulyaev YA. Agonist-induced Piezo1 activation suppresses migration of transformed
549 fibroblasts. Biochem Biophys Res Commun. 2019 Jun 18;514(1):173-179. doi:
550 10.1016/j.bbrc.2019.04.139.
551 24. Mousawi F, Peng H, Li J, Ponnambalam S, Roger S, Zhao H, Yang X, Jiang LH. Chemical
552 activation of the Piezo1 channel drives mesenchymal stem cell migration via inducing ATP
553 release and activation of P2 receptor purinergic signaling. Stem Cells. 2020 Mar;38(3):410-
554 421. doi: 10.1002/stem.3114.
555 25. Wang X, Cheng G, Miao Y, Qiu F, Bai L, Gao Z, Huang Y, Dong L, Niu X, Wang X, Li Y, Tang H,
556 Xu Y, Song X. Piezo type mechanosensitive ion channel component 1 facilitates gastric
557 cancer omentum metastasis. J Cell Mol Med. 2021 Feb;25(4):2238-2253. doi:
558 10.1111/jcmm.16217.
559 26. Gao L, Ji Y, Wang L, He M, Yang X, Qiu Y, Sun X, Ji Z, Yang G, Zhang J, Li S, Dai L, Zhang L.
560 Suppression of Esophageal Squamous Cell Carcinoma Development by Mechanosensitive
561 Protein Piezo1 Downregulation. ACS Omega. 2021 Apr 12;6(15):10196-10206. doi:
562 10.1021/acsomega.1c00505.
563 27. Holt JR, Zeng WZ, Evans EL, Woo SH, Ma S, Abuwarda H, Loud M, Patapoutian A, Pathak MM.
564 Spatiotemporal dynamics of PIEZO1 localization controls keratinocyte migration during
565 wound healing. Elife. 2021 Sep 27;10:e65415. doi: 10.7554/eLife.65415.

28. Velasco-Estevez M, Koch N, Klejbor I, Caratis F, Rutkowska A. Mechanoreceptor Piezo1 Is Downregulated in Multiple Sclerosis Brain and Is Involved in the Maturation and Migration of Oligodendrocytes in vitro. Front Cell Neurosci. 2022 May 26;16:914985. doi: 10.3389/fncel.2022.914985.
29. Hung WC, Yang JR, Yankaskas CL, Wong BS, Wu PH, Pardo-Pastor C, Serra SA, Chiang MJ, Gu Z, Wirtz D, Valverde MA, Yang JT, Zhang J, Konstantopoulos K. Confinement Sensing and Signal Optimization via Piezo1/PKA and Myosin II Pathways. Cell Rep. 2016 May 17;15(7):1430-1441. doi: 10.1016/j.celrep.2016.04.035.
30. McHugh BJ, Buttery R, Lad Y, Banks S, Haslett C, Sethi T. Integrin activation by Fam38A uses a novel mechanism of R-Ras targeting to the endoplasmic reticulum. J Cell Sci. 2010 Jan 1;123(Pt 1):51-61. doi: 10.1242/jcs.056424.
31. Xiao B. 2020. Levering Mechanically Activated Piezo Channels for Potential Pharmacological Intervention. Annu Rev PharmacolToxicol. 60:195-218. doi: 10.1146/annurev-pharmtox-010919-023703.
32. Barr VA, Bunnell SC. Interference reflection microscopy. Curr Protoc Cell Biol. 2009 Dec; Chapter 4: Unit 4.23. doi: 10.1002/0471143030.cb0423s45.
33. Chakraborty M, Mukherjee B, Nalinakshan N, Biswas A, Nayak RK, Sinha B. Effect of heterogeneous substrate adhesivity of follower cells on speed and tension profile of leader cells in primary keratocyte collective cell migration. Biol Open. 2022 Mar 15;11(3):bio058893. doi: 10.1242/bio.058893.
34. Mitra SK, Hanson DA, Schlaepfer DD. Focal adhesion kinase: in command and control of cell motility. Nat Rev Mol Cell Biol. 2005 Jan;6(1):56-68. doi: 10.1038/nrm1549.
35. Katoh K. FAK-Dependent Cell Motility and Cell Elongation. Cells. 2020 Jan 12;9(1):192. doi: 10.3390/cells9010192.
36. Yamashiro S, Watanabe N. A new link between the retrograde actin flow and focal adhesions. J Biochem. 2014 Nov;156(5):239-48. doi: 10.1093/jb/mvu053.
37. Martino F, Perestrelo AR, Vinarský V, Pagliari S, Forte G. Cellular Mechanotransduction: From Tension to Function. Front Physiol. 2018 Jul 5;9:824. doi: 10.3389/fphys.2018.00824.
38. Sánchez-Martín L, Sánchez-Sánchez N, Gutiérrez-López MD, Rojo AI, Vicente-Manzanares M, Pérez-Alvarez MJ, Sánchez-Mateos P, Bustelo XR, Cuadrado A, Sánchez-Madrid F, Rodríguez-Fernández JL, Cabañas C. Signaling through the leukocyte integrin LFA-1 in T cells induces a transient activation of Rac-1 that is regulated by Vav and PI3K/Akt-1. J Biol Chem. 2004 Apr 16;279(16):16194-205. doi: 10.1074/jbc.M400905200.

599 39. Roy NH, Kim SHJ, Buffone A Jr, Blumenthal D, Huang B, Agarwal S, Schwartzberg PL, Hammer
600 DA, Burkhardt JK. LFA-1 signals to promote actin polymerization and upstream migration in T
601 cells. J Cell Sci. 2020 Sep 9;133(17):jcs248328. doi: 10.1242/jcs.248328.
602 40. Ganguly D. Can Piezo2 substitute Piezo1 function in the context of T cell-specific deletion in
603 mice? Sci Adv, e-Letter published Sep 8, 2021, in response to Jairaman A et al.,
604 41. Chang JE, Buechler MB, Gressier E, Turley SJ, Carroll MC. Mechanosensing by Peyer's patch
605 stroma regulates lymphocyte migration and mucosal antibody responses. Nat Immunol.
606 2019 Nov;20(11):1506-1516. doi: 10.1038/s41590-019-0505-z.
607 42. Roy NH, MacKay JL, Robertson TF, Hammer DA, Burkhardt JK. Crk adaptor proteins mediate
608 actin-dependent T cell migration and mechanosensing induced by the integrin LFA-1. Sci
609 Signal. 2018 Dec 11;11(560):eaat3178. doi: 10.1126/scisignal.aat3178.
610 43. Limozin L, Sengupta K. Quantitative reflection interference contrast microscopy (RICM) in
611 soft matter and cell adhesion. Chemphyschem. 2009 Nov 9;10(16):2752-68.
612 44. Biswas A, Alex A, Sinha B. Mapping Cell Membrane Fluctuations Reveals Their Active
613 Regulation and Transient Heterogeneities. Biophys J. 2017 Oct 17;113(8):1768-1781. doi:
614 10.1016/j.bpj.2017.08.041.
615 45. Biswas A, Kashyap P, Datta S, Sengupta T, Sinha B. Cholesterol Depletion by MβCD Enhances
616 Cell Membrane Tension and Its Variations-Reducing Integrity. Biophys J. 2019 Apr
617 23;116(8):1456-1468.
618 46. Shiba H, Noguchi H, Fournier JB. Monte Carlo study of the frame, fluctuation and internal
619 tensions of fluctuating membranes with fixed area. Soft Matter. 2016 Feb 28;12(8):2373-80.
620 doi: 10.1039/c5sm01900a.

621

622

FIGURE LEGENDS

Figure 1. Piezo1 deficiency abrogates integrin-dependent motility in human T cells which is mediated through redistribution of Piezo1 at the leading edge in response to chemokine stimulation.

A. MSD versus time calculated for GFP^+ (potential Piezo1-knockdown cells) and GFP^- (potential control cells) in GFP plasmid and Piezo1 siRNA co-transfected human $CD4^+$ T lymphocytes, that were allowed to migrate in presence of recombinant CCL19 on ICAM1-coated dishes. **B.** Representative tracks of GFP^+ and GFP^- $CD4^+$ T lymphocytes. Comparisons of **C.** % GFP^+ cells after 72 hours of nucleofection **D & E.** 3D transwell migration assay of siRNA-transfected primary human $CD4^+$ T lymphocytes (D) and Jurkat T cells (E), respectively. Data representative of at least 3 independent experiments. **F.** Representative confocal images of Piezo1 distribution in fixed untreated and CCL19-treated $CD4^+$ T lymphocytes. 63X oil magnification. **G.** Comparison between Piezo1 polarity index calculated for fixed, stained, human $CD4^+$ T lymphocytes with or without 0.5µg/ml CCL19 treatment for 20-30 minutes. n > 510 random cells, each. **H.** Piezo1 polarity index calculated for Jurkat cells, expressing mCherry-tagged Piezo1 during live-cell tracking in the presence of recombinant SDF1α. Each dot represents polarity index of each cell, averaged over all the time-frames. **I.** Representative time kinetics of particle image velocimetry (PIV) analysis of Piezo1-mcherry transfected Jurkat cells, allowed to move on ICAM-coated dishes in the presence of recombinant SDF1α. Top panel: No chemokine. Bottom Panel: SDF1α.

Figure 2. Piezo1 redistribution in migrating T cells follow increased membrane tension in the leading edge

A. Schematic illustration of interference reflection microscopy imaging setup. **B.** Probability distribution of amplitude of temporal fluctuations (SD_{time}, left) and tension (right) before and after addition of chemokines. **C.** Temporal trajectory of tension of cells before and after addition of chemokine with ** indicating significant difference from control. **D.** Representative IRM images of Jurkat cells (top), corresponding tension maps (middle) and R^2 maps (bottom), before and after chemokine treatment. **E** Correlation between normalized Piezo intensity, tension magnitudes with time. **F.** Scatter plot to show correlation between normalized pixel count of Piezo1 and normalized tension. Piezo1 intensity at specific time-points were correlated with tension magnitudes at the preceding timepoints. Normalization has been done such that the maximum value is set to 1 and

655 others are accordingly scaled. **G.** Colour-coded Piezo1-GFP intensity map (left), epifluorescence
656 image (middle), and tension map (right) of representative Piezo1-GFP expressing Jurkat cell, after 30
657 minutes of 0.1µg/ml of SDF1α treatment.

658

659 **Figure 3. Focal adhesion following chemokine receptor activation does not depend on Piezo1**

660 **A.** Representative confocal images of human $CD4^+$ T lymphocytes, fixed and stained for phospho-FAK
661 (pFAK) under untreated and CCL19-treated conditions. **B.** Increased polarity of pFAK upon
662 chemokine stimulation of $CD4^+$ T lymphocytes as compared to unstimulated controls. N > 120 cells,
663 each. **C.** Representative confocal images of pFAK distribution in control and Piezo1 siRNA-transfected
664 $CD4^+$ T lymphocytes stimulated with chemokine. **D**. Comparison of pFAK polarity in CCL19-stimulated
665 control and Piezo1-knockdown $CD4^+$ T lymphocytes. n > 450 random cells, each. **E.** Representative
666 confocal images of stained Piezo1 in $CD4^+$ T cells stimulated with CCL19 in the presence or absence
667 of FAK inhibitor 14. **F.** Effect of FAK inhibition on Piezo1 polarity in $CD4^+$ T lymphocytes stimulated
668 with recombinant CCL19 versus untreated cells. n > 600 random cells, each. Data represented from
669 at least 3 independent experiments.

670

671 **Figure 4. Membrane recruitment of LFA1 on chemokine receptor activation disrupts with Piezo1**
672 **deficiency.**

673 **A.** Representative confocal images of fixed, immunostained Piezo1 and LFA1 in unstimulated and
674 CCL19-stimulated $CD4^+$ T lymphocytes. **B.** Increased LFA1 polarity in response to recombinant CCL19
675 stimulation in $CD4^+$ T cells. n > 295 random cells, each. **C.** Manders' co-localisation analysis of Piezo1
676 and LFA1 in untreated and CCL19-treated $CD4^+$ T lymphocytes. **D.** Comparison of LFA1 polarity in
677 chemokine-treated control and Piezo1 knockdown $CD4^+$ T lymphocytes. **E.** Representative confocal
678 stained images of LFA1 polarity of CCL19-treated control and Piezo1-knockdown $CD4^+$ T
679 lymphocytes. n > 490 random cells, each. **F.** Representative confocal images of phospho-Akt (pAkt)
680 and Akt distribution upon chemokine treatment of control and Piezo1-knockdown cells. **G & H.**
681 Quantitative analyses of pAkt (M) and Akt (N) polarity in control and Piezo1-knockdown cells after
682 CCL19-treatment. n > 580 random cells, each. Data represented from at least 3 independent
683 experiments.

684

685

Figure 5. Local Ca^{2+} mobilization with Piezo1 redistribution upon chemokine stimulation.

A. Representative TIRF image of a Jurkat Cell stained with Fluo3AM and transiently expressing with Piezo1 mCherry. Lower panel: zoomed in image and overlap of binary images of objects detected from Calcium and Piezo channels as well as simulated randomly placed punctas having similar total (in the zoomed in section) and average area as that of the Calcium punctas detected in the real images. Overlap RGB image shows the overlap between Real Calcium (Red) and piezo puncta (Green), overlap puncta (Yellow), simulated calcium puncta (blue). **B.** Comparison between percentage calcium colocalization of simulated data and real data. * Denote p value < 0.05 calculated using Mann Whitney U test. N cell= 52 (13 cells x 4 time points). NROIS= 52. **C.** Representative confocal images of LFA1 and actin distribution in CCL19-stimulated CD4+ T lymphocytes with or without inhibition of calpain. 100µM of PD15606 was added to the cells 1 hour prior to addition of chemokine. Quantitative comparisons of **D.** LFA1 and **E.** actin polarity upon chemokine stimulation, in the presence or absence of calpain pre-inhibition. N > 290 random cells, each.

Figure 6. Piezo1 deficiency disrupts F-actin retrograde flow in T cells despite chemokine receptor activation.

A. Representative fixed confocal images of actin and Piezo1 distribution in $CD4^+$ T lymphocytes after 30 mins of 0.5µg/ml recombinant CCL19 treatment. **B.** Quantitative comparison of actin polarity in control and Piezo1-knockdown $CD4^+$ T lymphocytes cells after 30 mins of chemokine treatment. n > 300 random cells, each. **C.** Representative fixed confocal images of actin distribution in chemokine-treated, control and Piezo1-knockdown $CD4^+$ T lymphocytes. Front-back (F/B) of Piezo1 and actin-GFP in SDF1α treated **(D)** and untreated **(E)** Jurkat cells co-expressing actin-GFP and Piezo1-mCherry. **F.** A snapshot of time-lapse imaging of Piezo1-mCherry and actin-GFP expressing Jurkat cell treated with 0.1µg/ml of SDF1α. Image is maximum Z-projection of the cell at 63X/1.40 magnification.

Figure 7. The mechanistic model depicting involvement of Piezo1 mechanosensing in leading edge events in a migrating T cell.

Proposed model suggests chemokine receptor activation in human T cells lead to focal adhesion kinase activation and focal adhesion formation. Focal adhesions lead to localized increase in

717 membrane tension at the leading edge plasma membrane which leads to Piezo1 recruitment and
718 activation. Piezo1 activation leads to calpain activation which potentially drives further cytoskeletal
719 consolidation to recruit integrin LFA1. LFA1 recruitment and activation lead to phosphorylation of
720 AKT and downstream signaling eventually driving the retrograde actin flow in migrating human T
721 cells.

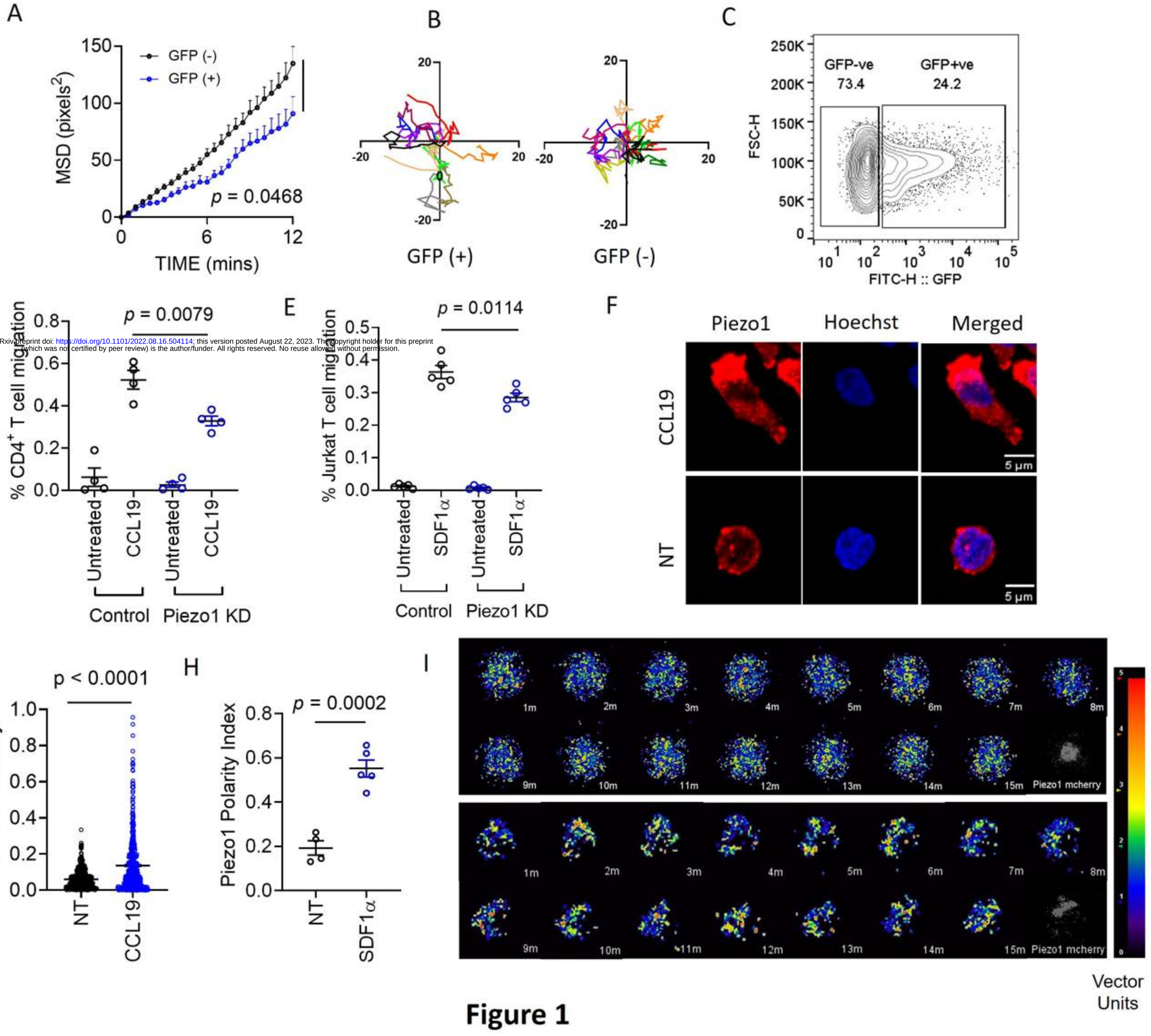

Figure 1

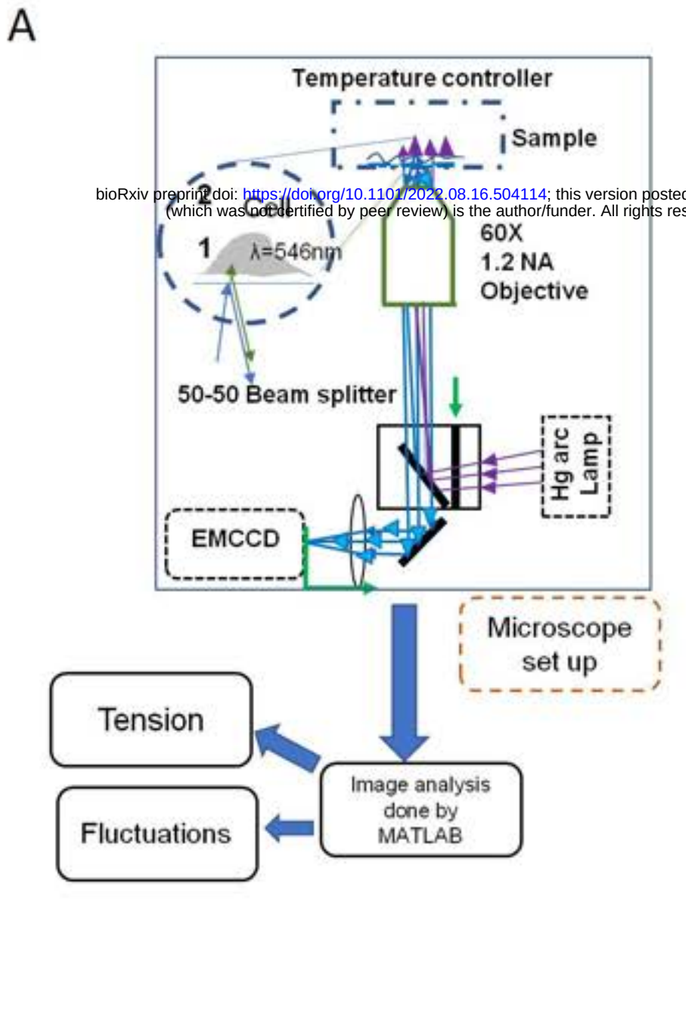

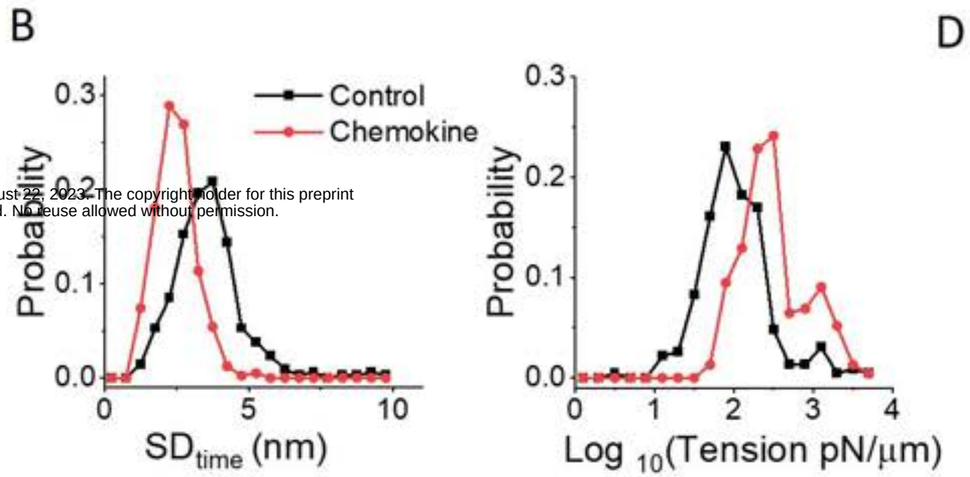

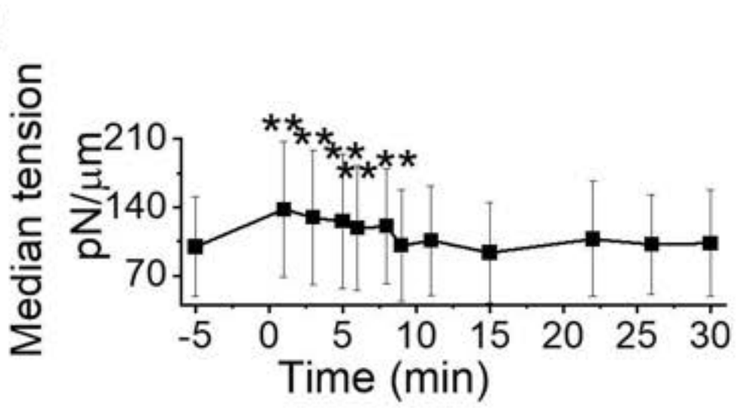

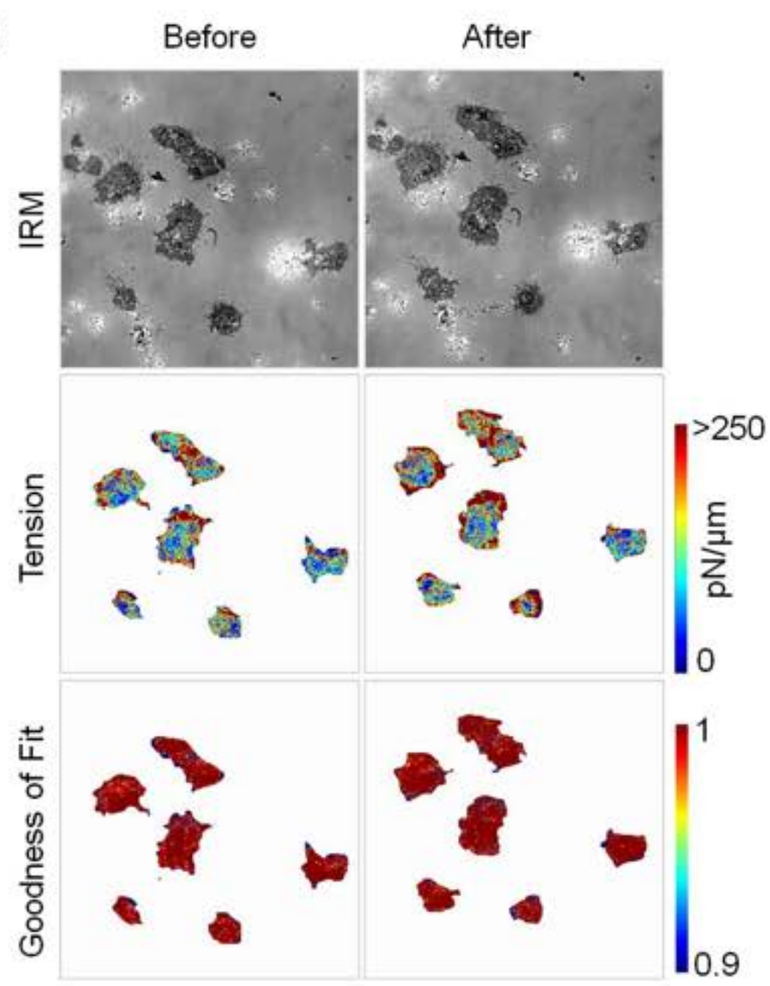

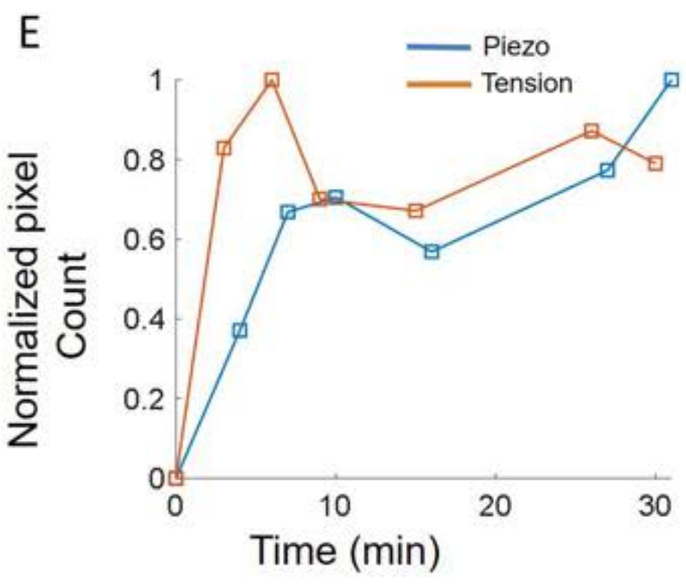

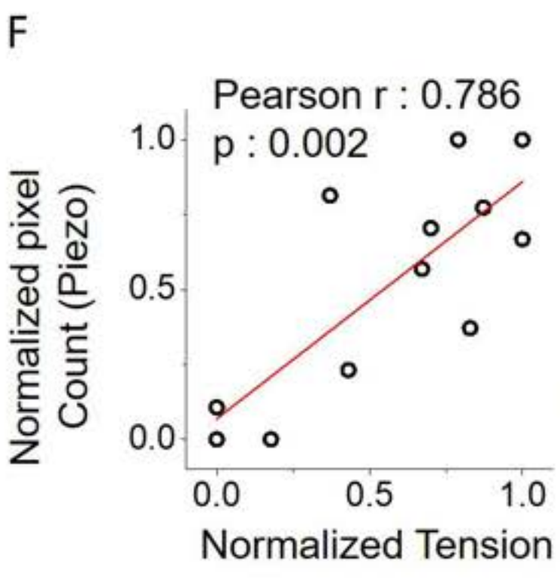

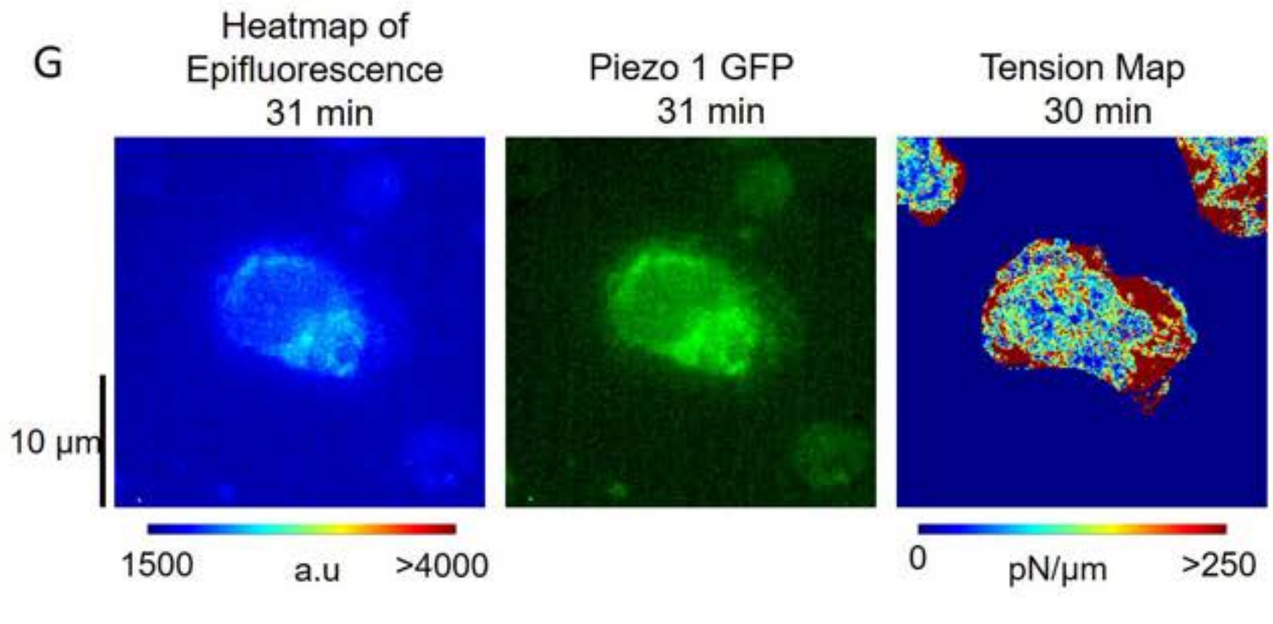

Figure 2

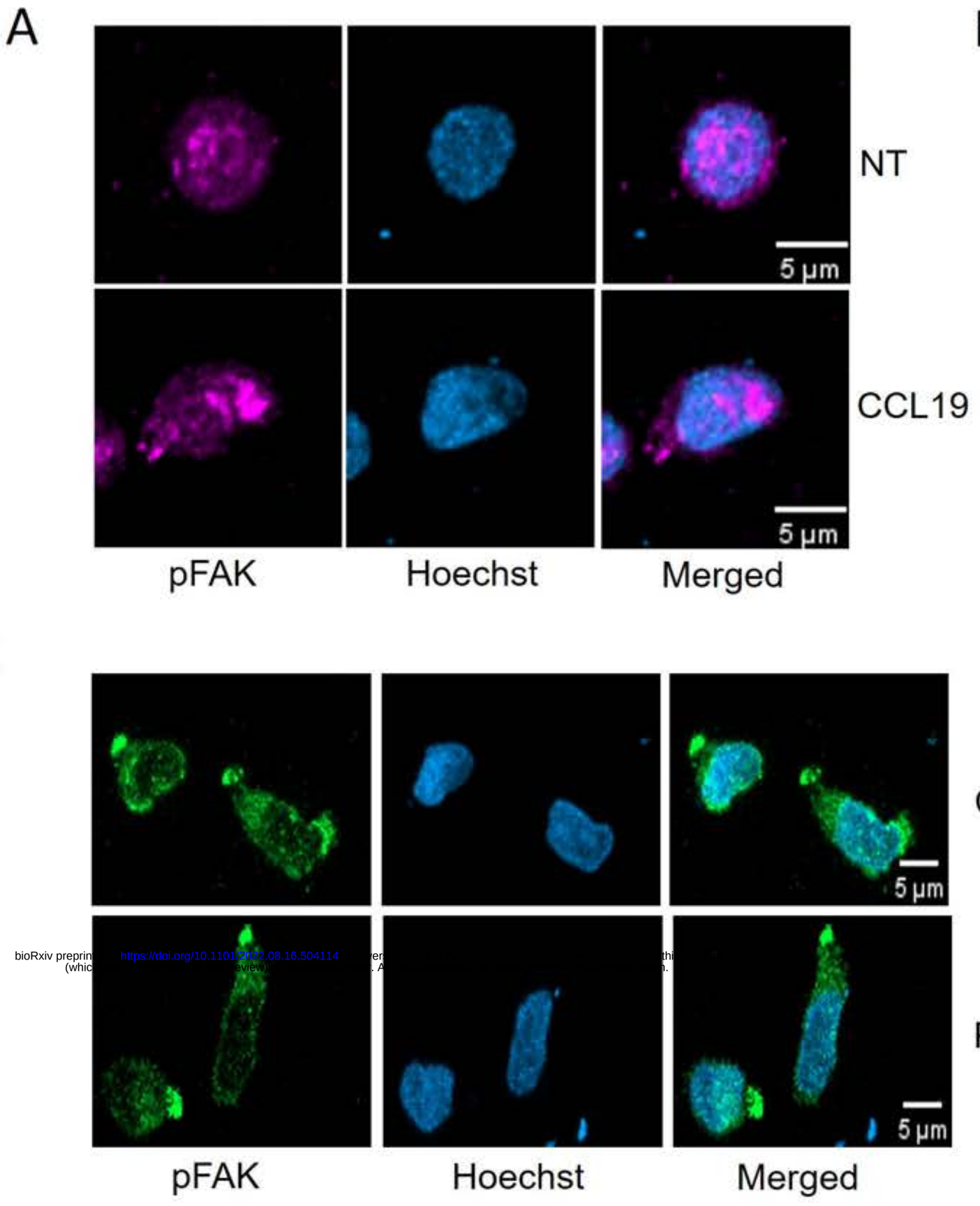

Figure 3

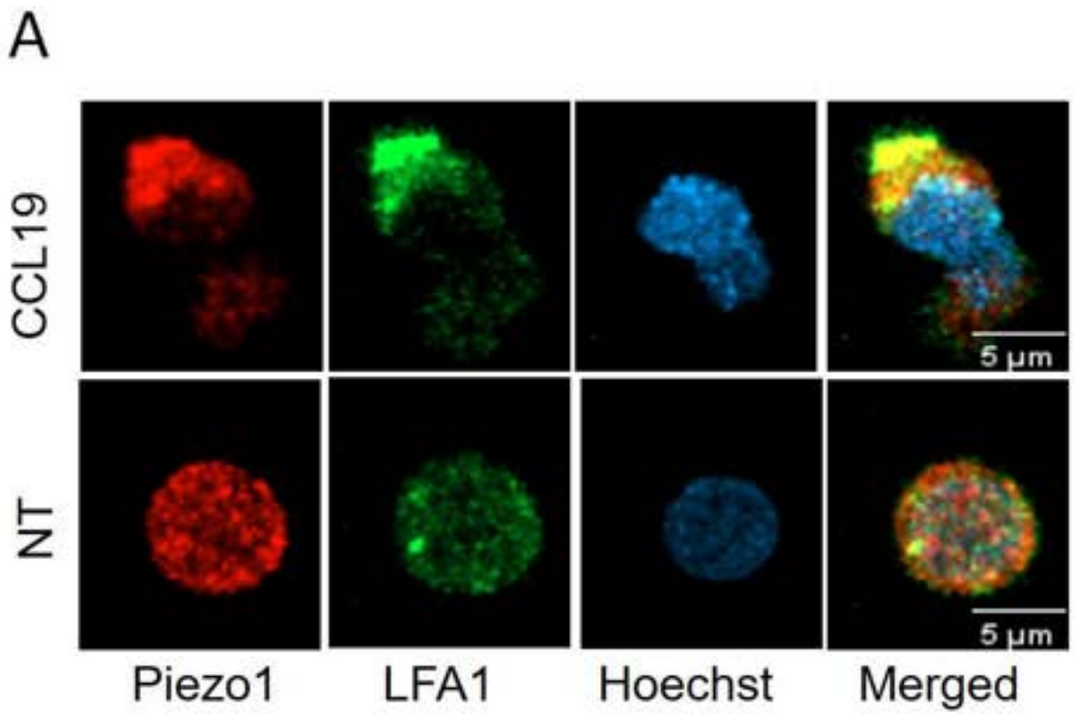

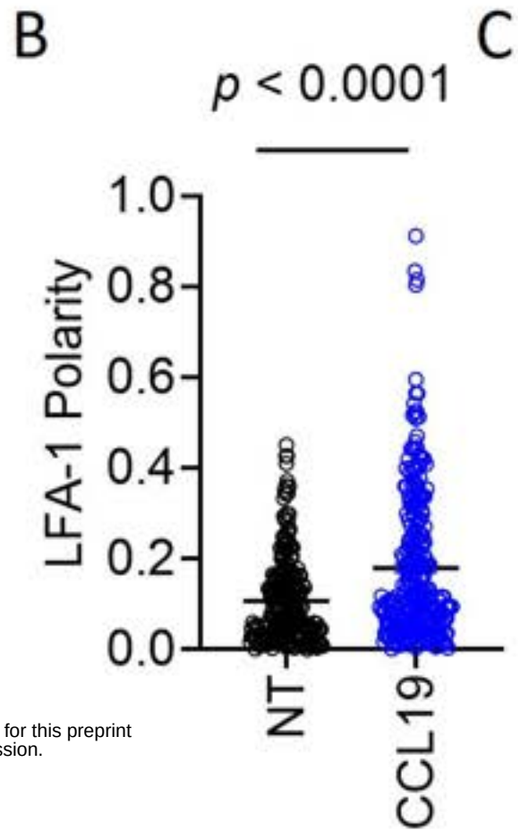

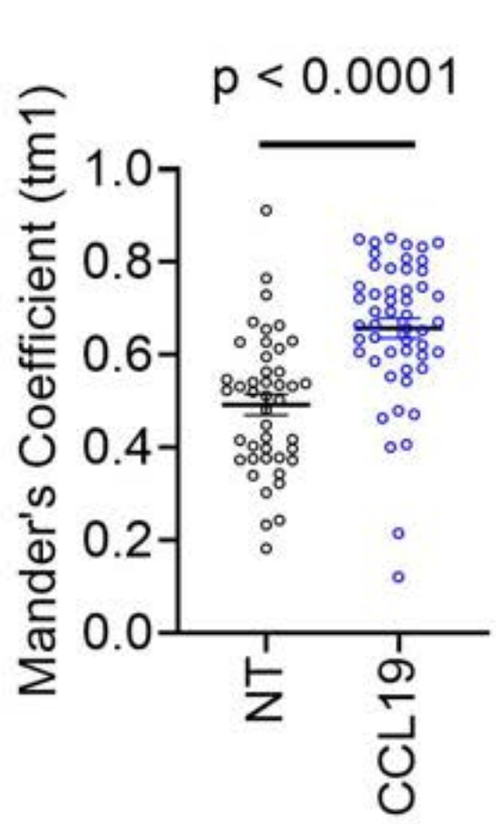

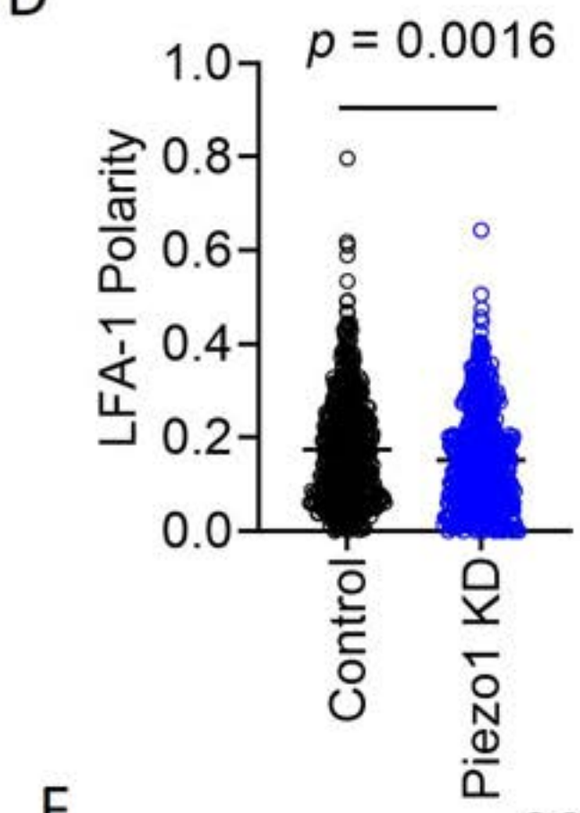

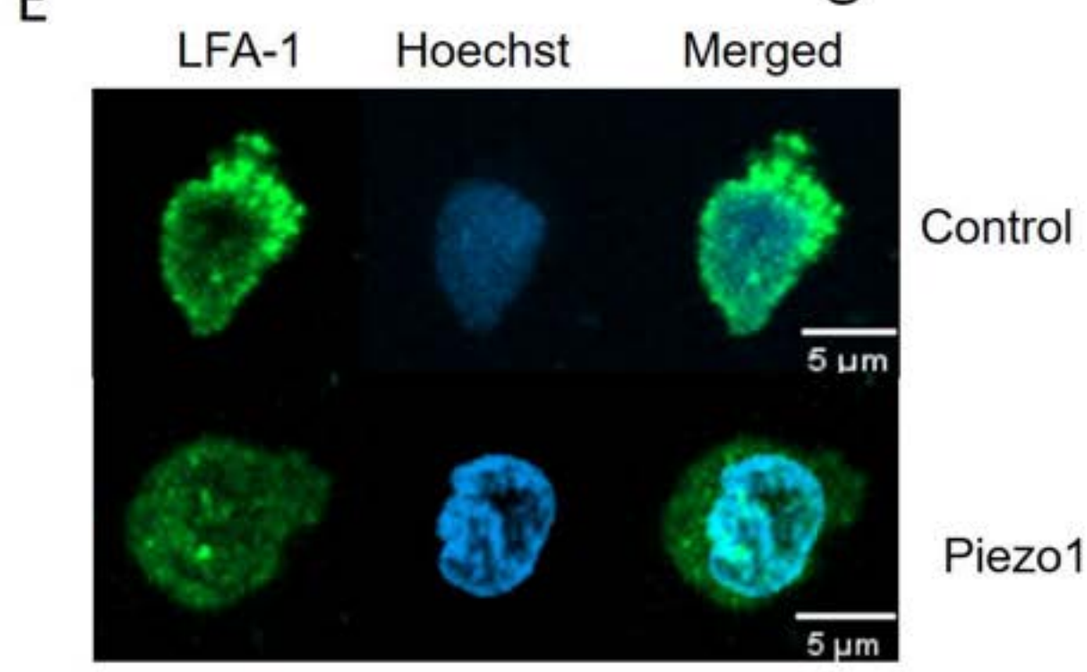

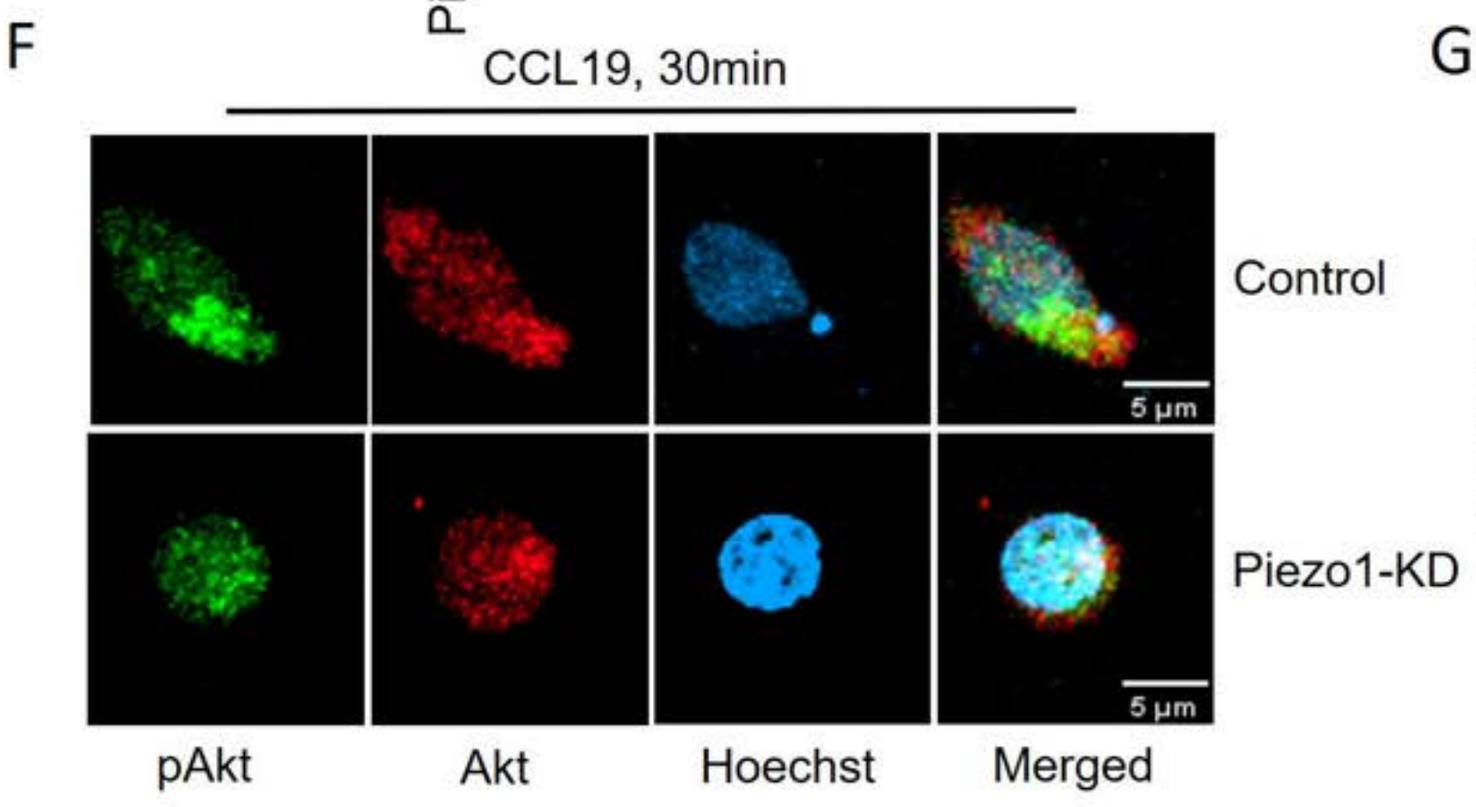

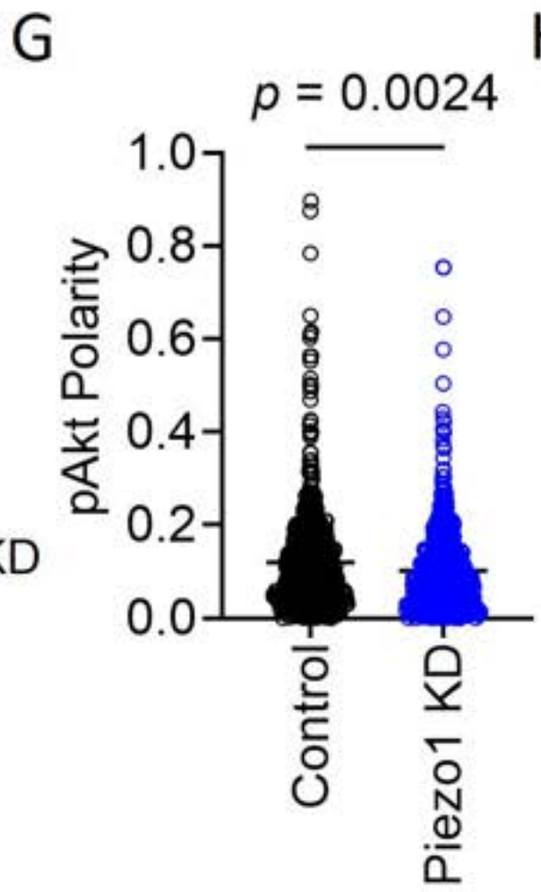

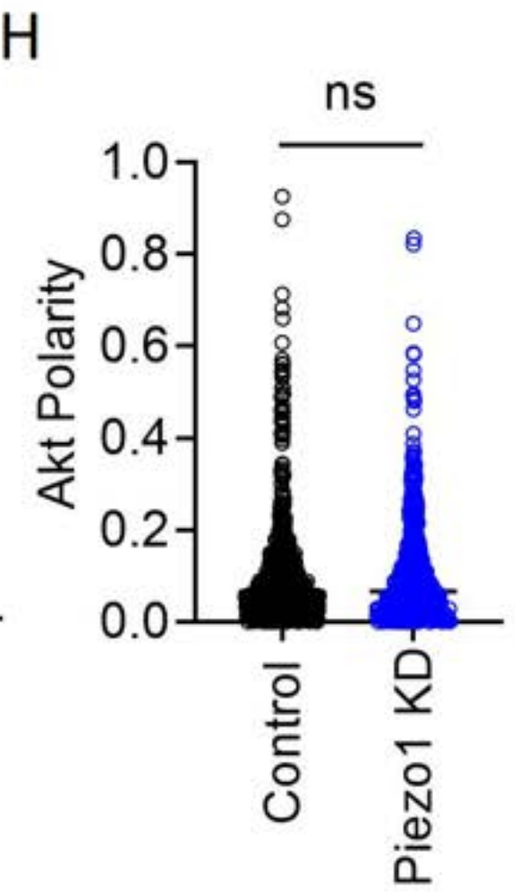

Figure 4

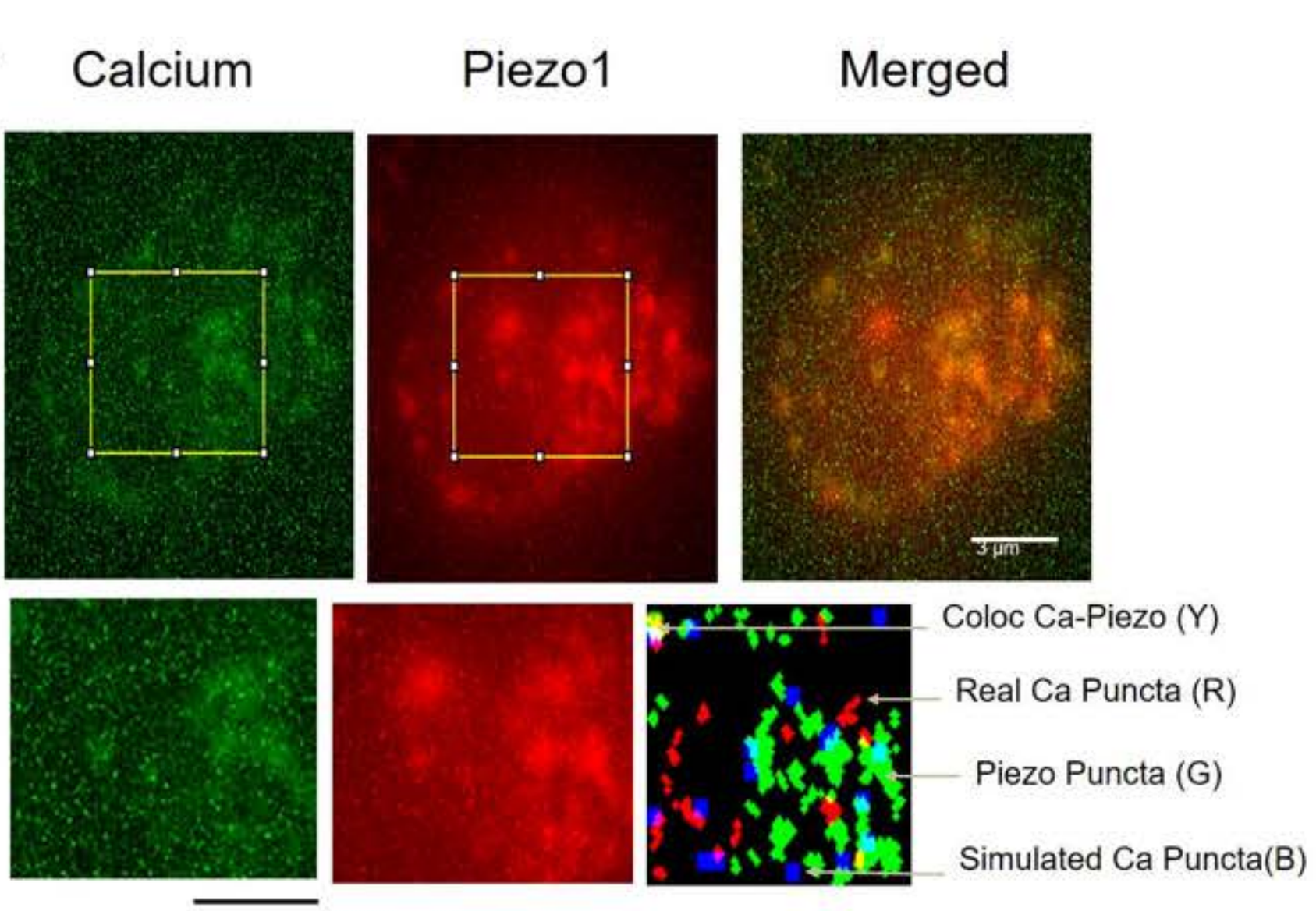

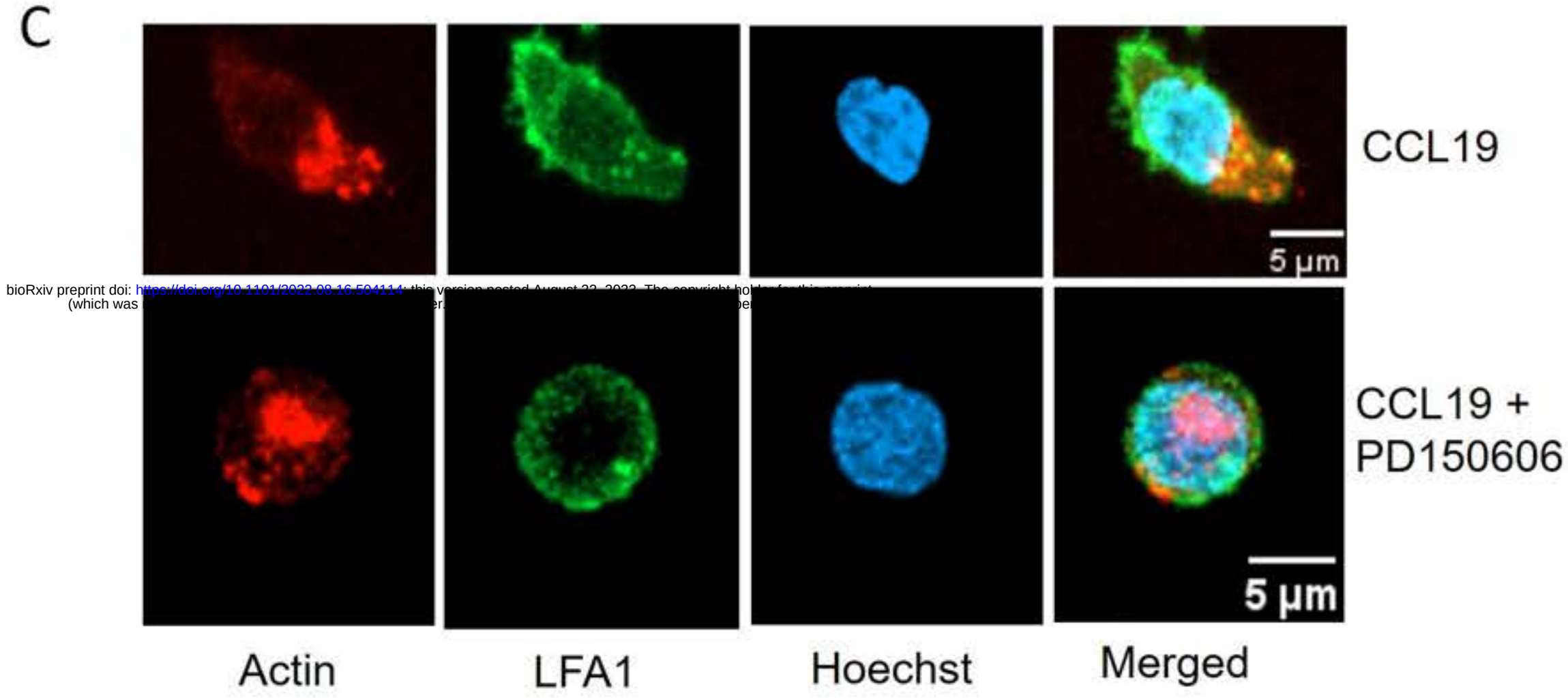

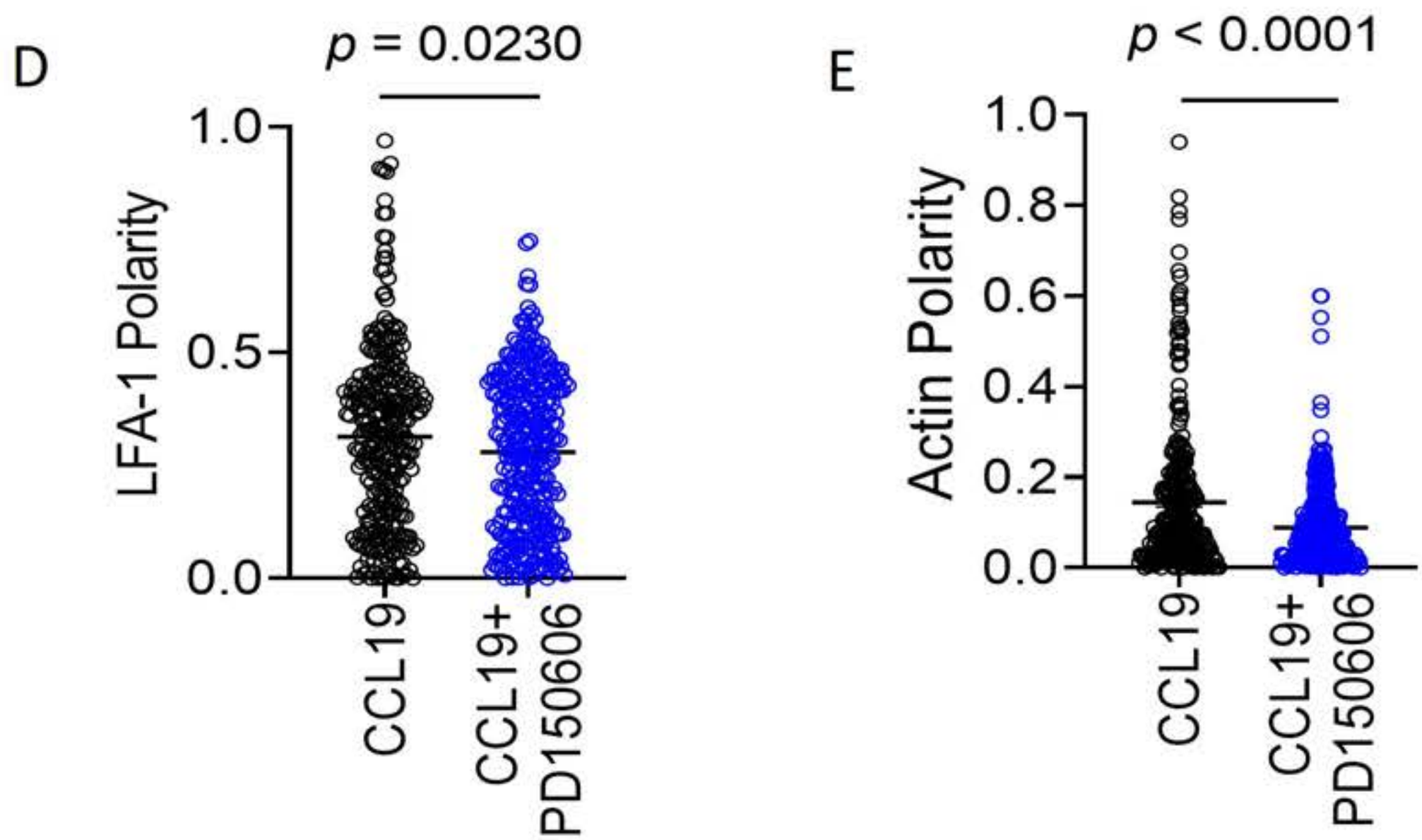

Figure 5

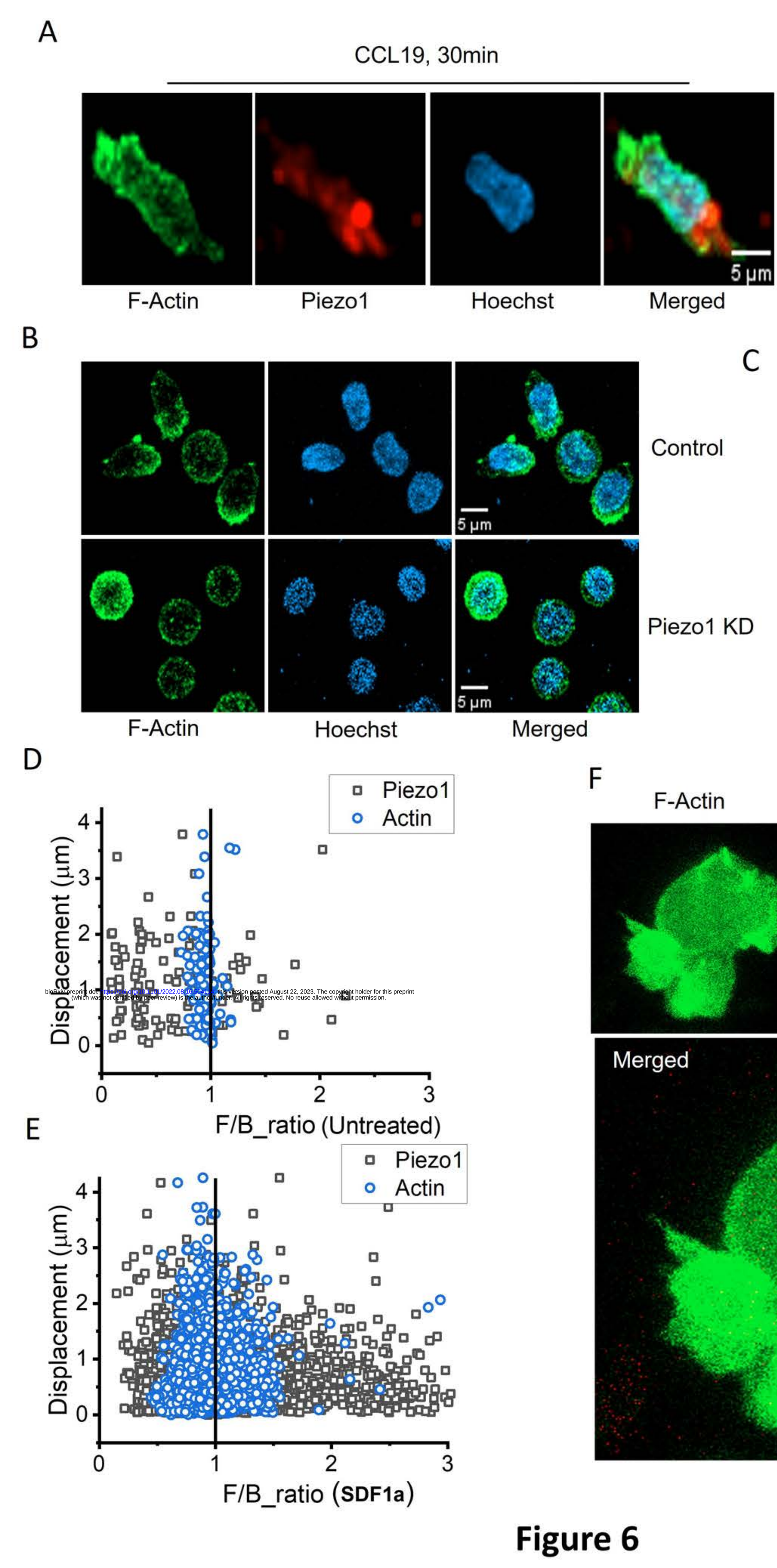

Figure 6

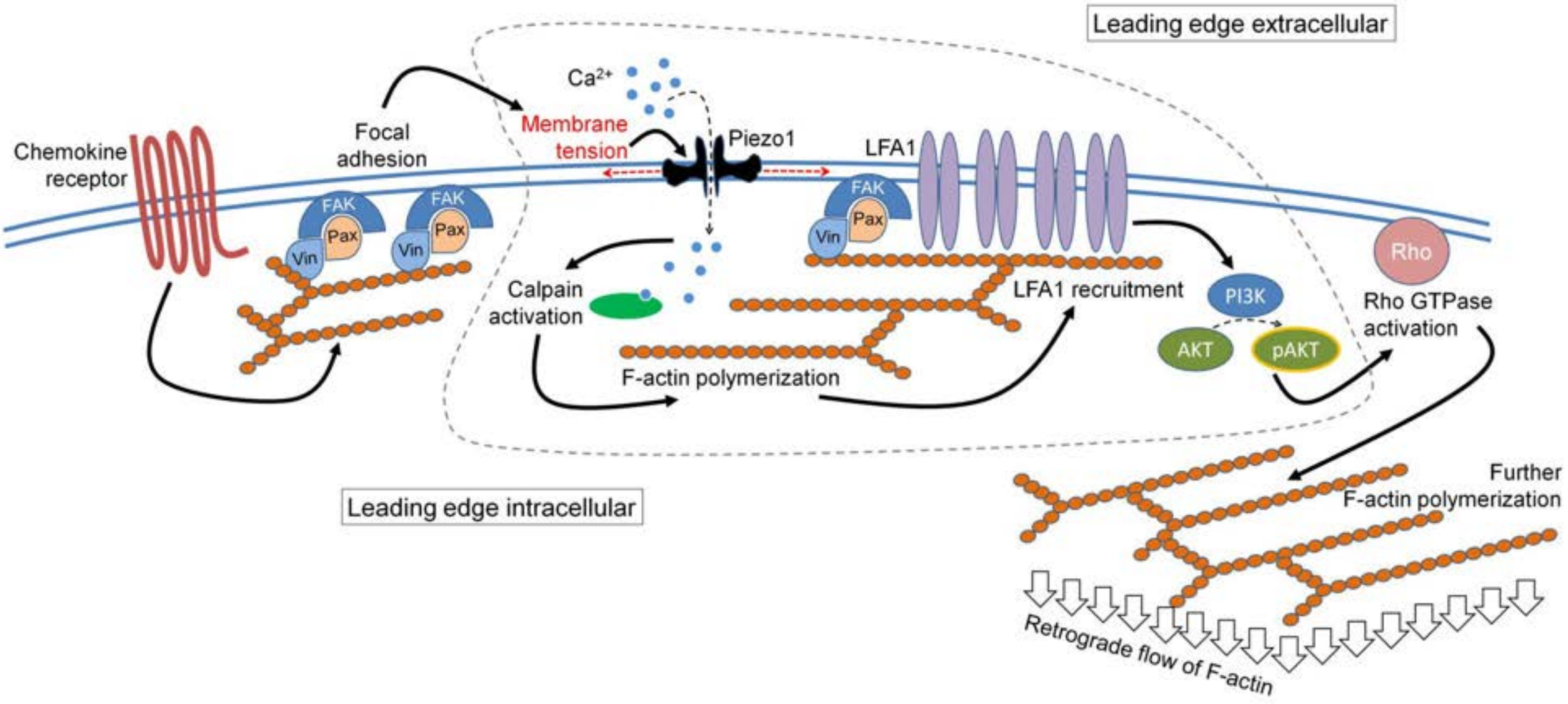
Leading edge extracellular
Ca2+
Membrane tension
Piezo1
Focal adhesion
Chemokine receptor
FAK
Pax
Vin
FAK
Pax
Vin
LFA1
FAK
Pax
Vin
Calpain activation
LFA1 recruitment
PI3K
AKT
pAKT
Rho
Rho GTPase activation
F-actin polymerization
Leading edge intracellular
Further F-actin polymerization
Retrograde flow of F-actin

Figure 7

Published January 12, 2018, doi:10.4049/jimmunol.1701118

Cutting Edge

The Journal of Immunology

Cutting Edge: Piezo1 Mechanosensors Optimize Human T Cell Activation

Chinky Shiu Chen Liu,[*,†] Deblina Raychaudhuri,[*,†] Barnali Paul,[‡] Yogaditya Chakrabarty,[§] Amrit Raj Ghosh,[*,†] Oindrila Rahaman,[*,†] Arindam Talukdar,[‡] and Dipyaman Ganguly[*,†]

TCRs recognize peptides on MHC molecules and induce downstream signaling, leading to activation and clonal expansion. In addition to the strength of the interaction of TCRs with peptides on MHC molecules, mechanical forces contribute to optimal T cell activation, as reflected by the superior efficiency of immobilized TCR–cross-linking Abs compared with soluble Abs in TCR triggering, although a dedicated mechanotransduction module is not identified. We found that the professional mechanosensor protein Piezo1 is critically involved in human T cell activation. Although a deficiency in Piezo1 attenuates downstream events on ex vivo TCR triggering, a Piezo1 agonist can obviate the need to immobilize TCR–cross-linking Abs. Piezo1-driven Ca^{2+} influx, leading to calpain activation and organization of cortical actin scaffold, links this mechanosensor to optimal TCR signaling. Thus, we discovered a hitherto unknown regulatory mechanism for human T cell activation and provide the first evidence, to our knowledge, for the involvement of Piezo1 mechanosensors in immune regulation. ***The Journal of Immunology*****, 2018, 200: 000–000.**

T cells are criticalCouncil of Scientific and Industrial Research– for adaptive immune response. $CD4^+$ and $CD8^+$ T cells are presented with cognate peptides (Ags) by APCs in the context of MHC class II and MHC class I, respectively, triggering TCR signaling and downstream activation events (1). A critical role for the affinity of the interaction between the TCR complex and peptide-bound MHC molecules (pMHCs) within the multicomponent immunological synapse is well established in the regulation of TCR signaling strength (1, 2).

In addition to the strength of TCR–pMHC interactions, the mechanical forces generated during this interaction seem to be important for efficient TCR triggering (3). Superior efficiency of ex vivo T cell activation and expansion by TCR–CD3 complex cross-linking using anti-CD3 Abs immobilized on microbeads or culture plates compared with soluble Abs alludes to a role for mechanical force–induced membrane perturbation in TCR triggering. Apposed T cell and APC membranes constrain movement dimensionality of the TCR–pMHC interaction, creating the possibility of vertical mechanical force on the cell membrane as a result of piston-like movements of interacting receptor complexes (2). Previous studies proposed intrinsic mechanosensing by the TCR–CD3 complex itself (4, 5). A specialized mechanosensor on the T cell membrane that regulates TCR activation by relaying mechanical cues had not been identified until now.

Piezo proteins are recently described conserved mechanosensitive channels (6, 7). Two Piezo proteins are described in vertebrates: Piezo1, which is involved in development, differentiation, and dynamics of various tissues (8–13), and Piezo2, which senses gentle touch (14, 15). Interestingly, Piezo proteins are widely expressed in immune cells, although their role in the regulation of the immune system is not known. Because of the notable expression of Piezo1 in human T cells, we explored the role of this professional mechanosensor in human T cell activation and identified that it functions as a specialized mechanotransducer that is critical for TCR triggering. Thus, we provide the first evidence, to our knowledge, for the important role of a Piezo protein in the regulation of the immune response.

Materials and Methods

Human T cell isolation and culture

PBMCs were collected from healthy donors with approval from the institutional review board and used for experiments. $CD4^+$ and $CD8^+$ T cells, isolated by magnetic immunoselection (Miltenyi Biotec), were treated with anti-CD3 and anti-CD28 Abs (2 μg/ml; eBioscience), anti-CD3/anti-

*IICB-Translational Research Unit of Excellence, Council of Scientific and Industrial Research–Indian Institute of Chemical Biology, Kolkata 700091, India; †Division of Cancer Biology and Inflammatory Disorders, Council of Scientific and Industrial Research–Indian Institute of Chemical Biology, Kolkata 700032, India; ‡Division of Organic and Medicinal Chemistry, Council of Scientific and Industrial Research–Indian Institute of Chemical Biology, Kolkata 700032, India; and §Division of Molecular Genetics, Council of Scientific and Industrial Research–Indian Institute of Chemical Biology, Kolkata 700032, India

ORCID: 0000-0002-7786-1795 (D.G.).

Received for publication August 7, 2017. Accepted for publication December 11, 2017.

This work was supported by a Ramanujan Fellowship from the Science and Engineering Research Board, India and by Grant BSC206 from the Council of Scientific and Industrial Research, India (to D.G.). C.S.C.L., D.R., B.P., and Y.C. received fellowships from the Council of Scientific and Industrial Research, India. A.R.G. and O.R. received fellowships from the University Grants Commission, India.

Address correspondence and reprint requests to Dr. Dipyaman Ganguly, IICB-Translational Research Unit of Excellence, Council of Scientific and Industrial Research–Indian Institute of Chemical Biology, CN6, Sector V, Salt Lake, Kolkata, West Bengal 700091, India. E-mail address: dipyaman@iicb.res.in

The online version of this article contains supplemental material.

Abbreviations used in this article: 3D, three dimensional; moDC, monocyte-derived dendritic cell; pMHC, peptide-bound MHC molecule; siRNA, small interfering RNA.

CD28 Dynabeads (1:1 cell/bead ratio; Thermo Fisher Scientific), and Yoda1 (15 μM). PD150606 (100 μM; Sigma-Aldrich) was used for calpain inhibition, and cyclosporine A (2.5 μM) was used for calcineurin phosphatase inhibition, as indicated. For allogeneic T cell proliferation, monocyte-derived dendritic cells (moDCs) were cocultured with T cells in a 1:5 moDC/T cell ratio for 4 d. moDCs were generated by culturing $CD14^+$ monocytes with human GM-CSF (50 ng/ml; eBioscience) and IL-4 (50 ng/ml; Tonbo) for 4 d. In autologous T cell–proliferation experiments, moDCs were primed with 2 IU/ml tetanus toxoid (Serum Institute India) for 24 h before coculture with $CD45RA^-$ $CD4^+$ T cells in a 1:5 or 1:10 moDC/T cell ratio. Coculture with unprimed moDCs was used as control.

RNA interference

Piezo1 knockdown was performed in freshly isolated T cells by electroporating 150 nM Piezo1-targeting small interfering RNA (siRNA) or control EGFP–targeting siRNA (MISSION esiRNA; Sigma-Aldrich). The cells were cultured for 3 d before functional studies. Statistical validation of functional differences was done in experiments that achieved ≥40% re-

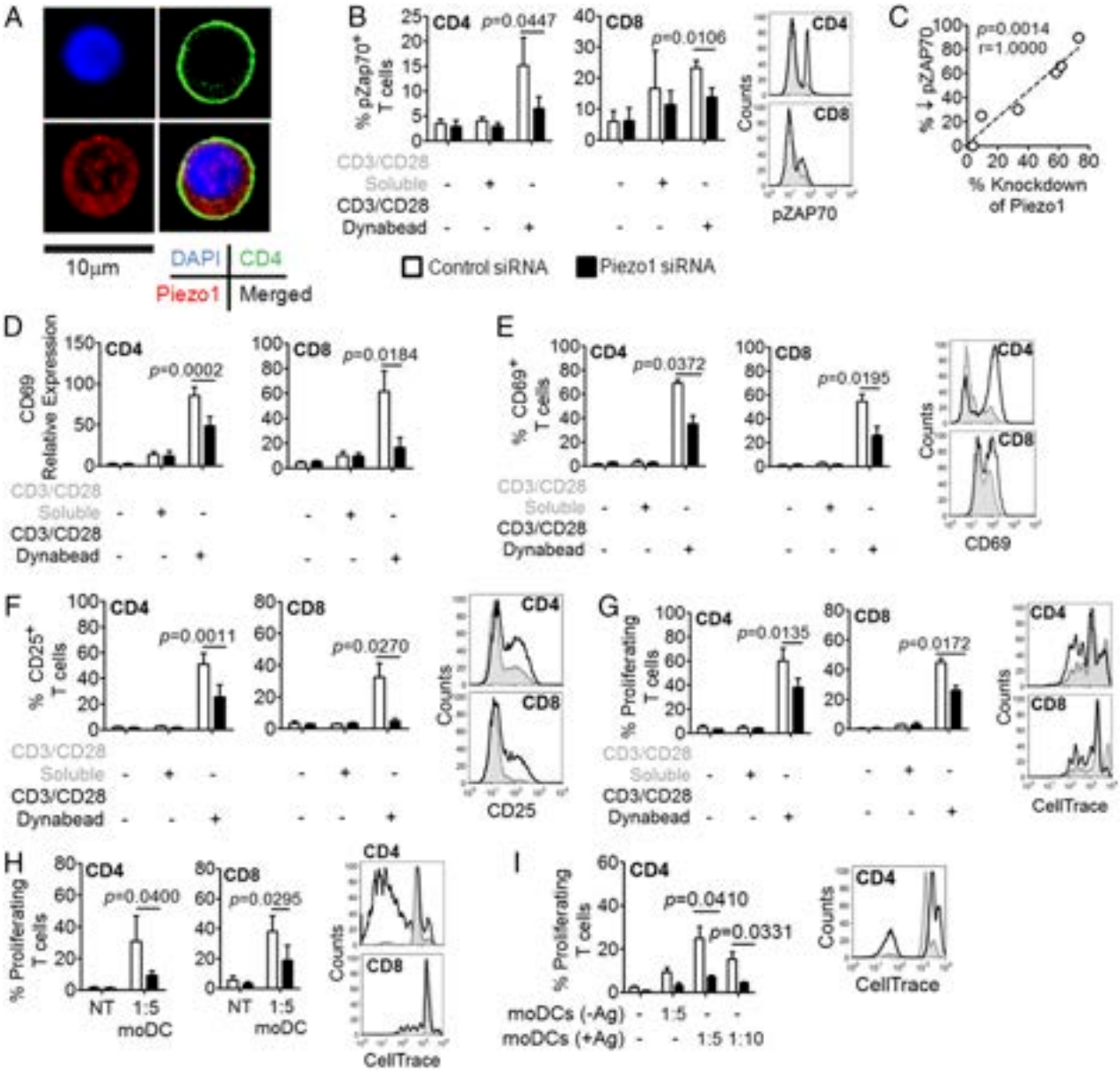

FIGURE 1. Piezo1 is essential for optimal human T cell activation. (**A**) Confocal microscopy image of resting $CD4^+$ T cells. (**B**) Phospho-ZAP70 was assessed by flow cytometry in T cells in response to stimulation with soluble or bead-immobilized anti-CD3/anti-CD28 Abs at 1 h (left and middle panels). Representative flow cytometry line graphs (right panels). Black line, control siRNA; shaded area, Piezo1 siRNA. (**C**) Correlation between the extent of reduction in Piezo1 expression due to RNA interference and the reduction in phospho-ZAP70. Spearman correlation coefficient (r) and *p* value are indicated. (**D**) CD69 gene expression was assessed in T cells in response to stimulation at 1 h. (**E**) Surface CD69 level was assessed by flow cytometry in T cells in response to stimulation at 18 h (left and middle panels). Representative line graphs (right panels). (**F**) Surface expression of CD25 was assessed by flow cytometry in T cells in response to stimulation at 36 h (left and middle panels). Representative line graphs (right panels). (**G**) Cellular proliferation was assessed by flow cytometry in siRNA-transfected $CD4^+$ and $CD8^+$ T cells in response to stimulation after 4 d (left and middle panels). Representative line graphs (right panels). (**H**) Cellular proliferation was assessed by flow cytometry in T cells, after 4 d of coculture with allogeneic moDCs at a 1:5 moDC/T cell ratio (left and middle panels). Representative line graphs (right panels). (**I**) Cellular proliferation was assessed by flow cytometry in $CD4^+$ T cells, after 4 d of coculture with autologous moDCs (at the indicated moDC/T cell ratio) loaded with tetanus toxoid (left panel). Representative line graph (right panel). Data from at least three independent experiments are presented, unless specified otherwise. The *p* values were calculated using a Student *t* test.

duction in Piezo1 expression. Immunoblot analysis of Piezo1 was performed after 72 h of siRNA transfection using an anti-Piezo1 Ab (1:500; Santa Cruz Biotechnology).

RNA isolation and quantitative real-time PCR

Total RNA was isolated from cells using TRIzol Reagent (Thermo Fisher Scientific), and real-time PCR was performed for the indicated genes following established methods, using 18s rRNA gene as control.

Flow cytometry

Anti–phospho-ZAP70–PE (eBioscience), CD69-PE, CD25-allophycocyanin, CD4-allophycocyanin, and CD8-allophycocyanin (BD Biosciences) were used for functional studies on T cells. Proliferation was assessed using CellTrace dye (Thermo Fisher Scientific). For quantitation of F-actin content, cells were fixed (4% paraformaldehyde), permeabilized (0.1% saponin), and stained with Alexa Fluor 532–labeled phalloidin (1:500; Thermo Fisher Scientific). For Ca^{2+} influx kinetics, cells were stained with Fluo-3, AM (5 μM; Sigma-Aldrich). Incubation with 1 mM EGTA was done for 1 h, as indicated.

Chemical synthesis of Yoda1

The synthesis of Yoda1 was done as per the scheme shown in Supplemental Fig. 1A. its purity was assessed by [^{1}H] nuclear magnetic resonance in $CDCl_3$ (Supplemental Fig. 1B) and [^{13}C] nuclear magnetic resonance in $CDCl_3$ (Supplemental Fig. 1C), as well as by electron ionization high-resolution mass spectrometry (Supplemental Fig. 1D).

Confocal microscopy

For Piezo1 localization, fixed (4% paraformaldehyde) and permeabilized (acetone) cells were stained with goat anti-human Piezo1 (1:25 dilution; Santa Cruz Biotechnology) for 1 h, followed by Alexa Fluor 647–labeled anti-goat secondary (Thermo Fisher Scientific) and anti-CD4–PE. Images were acquired using a Leica TCS SP8 confocal microscope. Total versus central distribution of Piezo1 was assessed by measuring the intensity of two concentric areas for each cell. The total/central fluorescence ratio was calculated using ImageJ for ≥100 cells from multiple fields. To assess the cortical actin scaffold, $CD4^+$ T cells were fixed, permeabilized, and stained with Alexa Fluor 532–phalloidin (1:100; Thermo Fisher Scientific) for 30 min. We used an Olympus IX81 microscope with a Yokogawa CSU-X1 spinning disc system. For three-dimensional (3D) confocal imaging, requisite image stacks (0.25-μm Z-steps) were acquired. Imaris 7 (Bitplane) was used for 3D reconstruction and volume rendering after Gaussian filtering. Twenty-five to fifty cells from multiple microscopic fields were analyzed.

Statistical analysis

A paired or unpaired Student *t* test was performed, as indicated in the figure legends, for statistical validation of data. All data are represented in the figures as mean ± SEM.

Results and Discussion

Piezo1 is essential for optimal TCR activation

First, we determined whether Piezo proteins are expressed in human T cells. We found that Piezo1 is expressed in human T cells but Piezo2 is not (Supplemental Fig. 2A), with resting distribution in intracellular vesicles and plasma membrane (Fig. 1A). To assess whether these professional mechanosensors play any role during TCR activation, signature early-activation events (i.e., expression of CD69 and phosphorylation of ZAP70), as well as longer-term outcomes like CD25 expression and proliferation, were determined after TCR cross-linking with anti-CD3 and anti-CD28 Abs. As expected, soluble Abs were much less efficient in TCR activation compared with Abs immobilized on beads. We made human T cells deficient in Piezo1 expression by RNA interference. In response to bead-immobilized anti-CD3 and anti-CD28 Abs, Piezo1-deficient (>40% reduction, Supplemental Fig. 2B, 2C) $CD4^+$ and $CD8^+$ T cells failed to achieve optimal TCR activation. Piezo1-deficient T cells showed significant reductions in phosphorylation of ZAP70 (Fig. 1B), induction of CD69 transcripts (Fig. 1D), and surface expression of CD69 (Fig. 1E). Phosphorylation of ZAP70 in response to TCR activation had a strong linear correlation with the relative abundance of Piezo1 transcripts in the T cells (Fig. 1C). Surface expression of the activation marker CD25 (Fig. 1F) and cellular proliferation (Fig. 1G) on TCR activation were also significantly reduced in Piezo1-deficient T cells.

Piezo1 deficiency impairs priming of T cells by APCs

To determine whether Piezo1 on T cells plays a role in efficient priming by APCs, we performed ex vivo assays for allogeneic and autologous Ag presentation. When transfected with Piezo1 siRNA, T cells were less responsive to priming by allogeneic moDCs, in terms of proliferation (Fig. 1H). For autologous priming, we cocultured effector $CD4^+$ T cells from tetanus-immunized donors with autologous moDCs that were loaded with tetanus toxoid, and found that Piezo1-deficient T cells failed to proliferate (Fig. 1I). Thus, the contribution of the Piezo1 mechanosensor to optimal TCR activation is critical during Ag priming of T cells by APCs, pointing to the physiological relevance of this mechanosensor in the immune response.

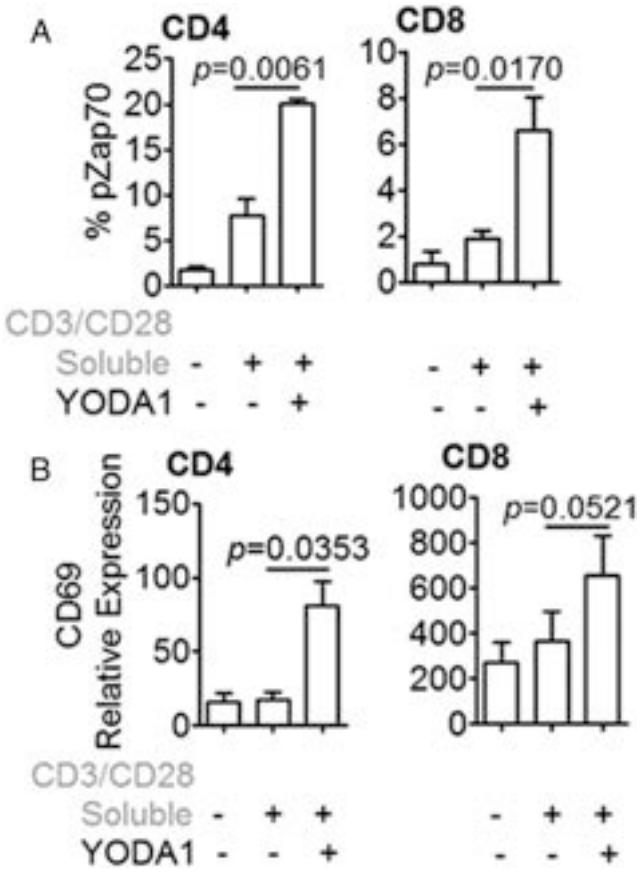

FIGURE 2. The Piezo1 agonist Yoda1 potentiates TCR triggering in response to soluble Abs. (**A**) Phospho-ZAP70 was assessed by flow cytometry in T cells in response to soluble anti-CD3/anti-CD28 Abs in the absence or presence of Yoda1 at 1 h. (**B**) Relative abundance of CD69 transcripts in comparison with 18s rRNA transcripts in T cells in response to soluble anti-CD3/anti-CD28 Abs in the absence or presence of Yoda1 at 1 h, as determined by real-time PCR.

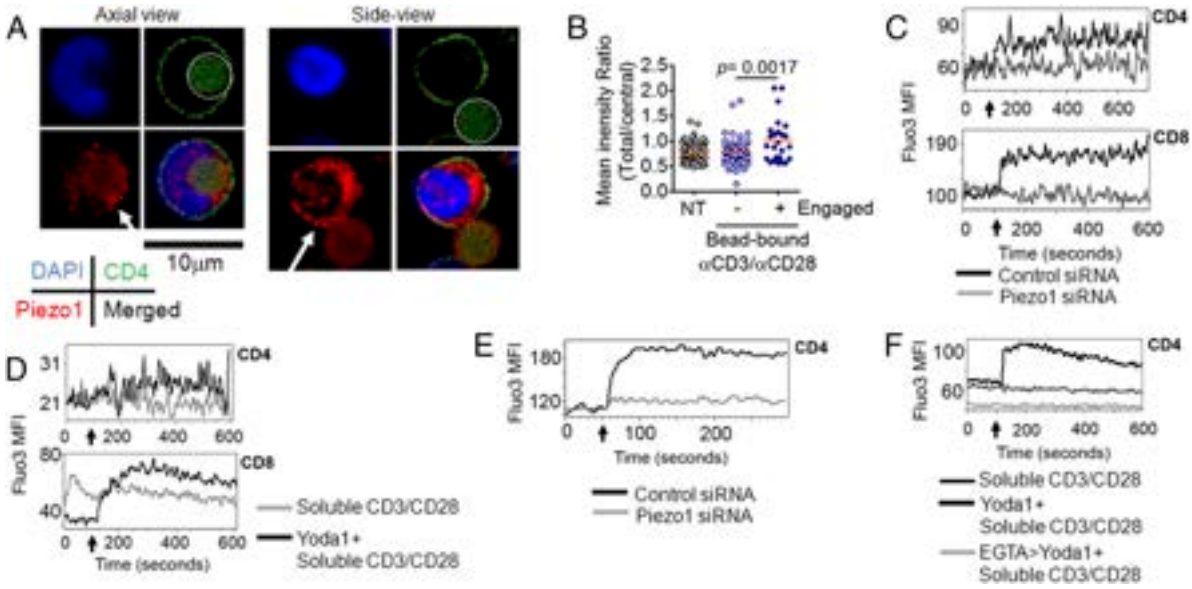

FIGURE 3. Membrane-recruited Piezo1 drives intracellular Ca^{2+} influx on human TCR activation. (**A**) Representative confocal images of $CD4^+$ T cells engaged with beads, with immobilized anti-CD3/anti-CD28 Abs showing a peripheral distribution around the synapse (white arrows). Axial view of a cell–bead conjugate (left panels). Side view (right panels) Dashed lines denote the beads. (**B**) Comparison of total and central Piezo1 staining in $CD4^+$ T cells; an increase in this ratio signifies more peripheral distribution of Piezo1. (**C**) Representative flow cytometry plots (Fluo-3, AM fluorescence) of intracellular Ca^{2+} influx in response to bead-immobilized Abs in T cells. Arrows denote the addition of beads. (**D**) Representative flow cytometry kinetics plots (Fluo-3, AM fluorescence) of intracellular Ca^{2+} influx in T cells in response to soluble Abs in the absence or presence of Yoda1. Arrows denote the addition of Abs, with or without Yoda1. (**E**) Representative flow cytometry kinetics plots (Fluo-3, AM fluorescence) of intracellular Ca^{2+} influx in response to soluble Abs and Yoda1 in Piezo1 siRNA–transfected $CD4^+$ T cells compared with control siRNA–transfected cells. Arrow denotes the addition of Abs+Yoda1. (**F**) Representative flow cytometry kinetics plots (Fluo-3, AM fluorescence) of intracellular Ca^{2+} influx in response to soluble Abs and Yoda1 in $CD4^+$ T cells in the absence or presence of EGTA. Arrow denotes the addition of Abs, with or without Yoda1.

Piezo1 agonists potentiate TCR activation by Ab cross-linking

We wanted to validate the contribution of Piezo1 to optimal TCR activation in the presence of a chemical surrogate for mechanical force. Yoda1 is a chemical agonist that activates Piezo1 independently of mechanical cues or any other cellular component (16). We found that addition of Yoda1 enabled soluble anti-CD3/anti-CD28 Abs to induce optimal TCR activation in $CD4^+$ and $CD8^+$ T cells, in terms of phosphorylation of ZAP70 (Fig. 2A), as well as induction of CD69 transcripts (Fig. 2B). Thus, chemical activation of Piezo1 obviated the need to immobilize the cross-linking Abs for optimal TCR triggering. Yoda1 activity was dependent on Piezo1, because an increase in CD69 expression in response to Yoda1 added with soluble anti-CD3/anti-CD28 was abrogated in Piezo1-deficient $CD4^+$ T cells (Supplemental Fig. 2D). The continued presence of Yoda1 was detrimental to cellular health, preventing assessment of later outcomes of activation (data not shown).

Calcium influx and calpain activation mediate Piezo1 function in T cell activation

We found on engagement with anti-CD3/anti-CD28 beads that Piezo1 showed more peripheral distribution around the synapse (Fig. 3A, 3B). Piezo1 mechanosensors are cation channels that mediate the influx of extracellular calcium on activation (17). In T cells, as well, TCR cross-linking by bead-immobilized anti-CD3/anti-CD28 Abs leads to rapid Ca^{2+} influx. In $CD4^+$ and $CD8^+$ T cells (Fig. 3C), Piezo1 deficiency largely abolishes this Ca^{2+} influx. Accordingly, in response to soluble anti-CD3/anti-CD28 Abs, appreciable Ca^{2+} influx could only be measured in the presence of the Piezo1 agonist Yoda1 (Fig. 3D). As expected, soluble anti-CD3/anti-CD28 Ab–induced Ca^{2+} influx in the presence of Yoda1 was abolished in Piezo1-deficient T cells (Fig. 3E). This Yoda1-induced Ca^{2+} influx was largely abolished in the presence of the cell-impermeable Ca^{2+} chelator EGTA as well, indicating extracellular sourcing of Ca^{2+} (Fig. 3F).

Cytosolic Ca^{2+} acts as a second messenger potentiating downstream receptor signaling. Among the Ca^{2+}-responsive enzymes that are involved in immediate outcomes of T cell activation (18), inhibition of the cysteine protease calpain (by PD150606) abolished optimal TCR activation (quantified by CD69 expression) in the presence of Yoda1 (Fig. 4A), as opposed to calcineurin phosphatase (Fig. 4B). The proteolytic function of calpain is critical for cytoskeletal rearrangements by actin reorganization (19, 20), which is essential for stabilization of the immunological synapse and effective T cell activation (21–23). Accordingly, we found, using flow cytometry, that the increased F-actin content of $CD4^+$ T cells (21), in response to soluble anti-CD3/anti-CD28 Abs supplemented with Yoda1 (Fig. 4C, Supplemental Fig. 2E), was inhibited in the presence of a calpain inhibitor. Calpain-dependent organization of the cortical actin scaffold in response to Piezo1 activation was also evident upon confocal microscopy of T cells (Fig. 4D, 4E). A significant increase in F-actin content was noted in response to bead-immobilized anti-CD3/anti-CD28 Abs as well (Supplemental Fig. 2F), which was abrogated in Piezo1-deficient $CD4^+$ T cells (Supplemental Fig. 2F, 2G). As expected, Piezo1 markedly colocalized with the F-actin scaffold beneath the immune

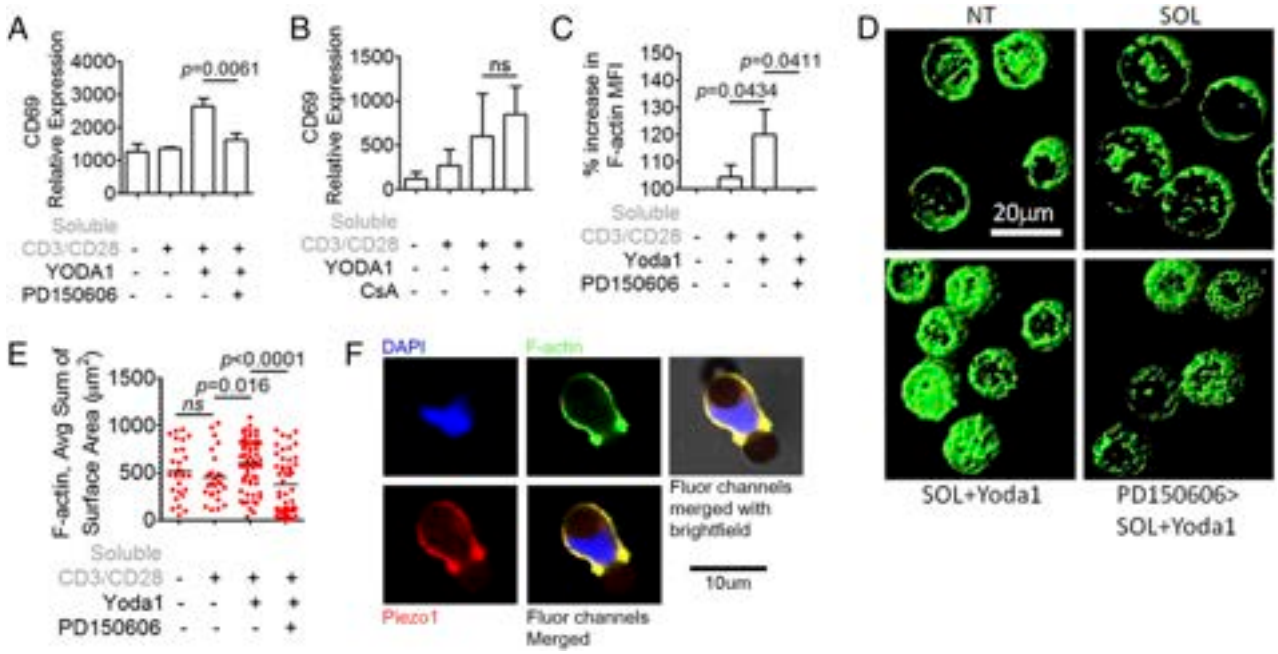

FIGURE 4. Piezo1-driven Ca^{2+} influx leads to calpain activation and organization of a cortical actin scaffold during human T cell activation. (**A**) CD69 gene expression was assessed in $CD4^+$ T cells in response to soluble anti-CD3/anti-CD28 Abs, in the absence or presence of Yoda1 and the calpain inhibitor PD150606 at 1 h. (**B**) CD69 gene expression was assessed in $CD4^+$ T cells in response to soluble anti-CD3/anti-CD28 Abs, in the absence or the presence of Yoda1 and the calcineurin phosphatase inhibitor cyclosporine A (CsA) at 1 h. (**C**) Flow cytometric assessment of F-actin content in $CD4^+$ T cells in response to soluble anti-CD3/anti-CD28 Abs, in the absence or presence of Yoda1 and the calpain inhibitor PD150606 at 30 min. Data from at least three independent experiments are represented in every experiment. (**D**) Cortical actin scaffold organization was assessed by confocal microscopy in $CD4^+$ T cells in response to soluble anti-CD3/anti-CD28 Abs, in the absence or presence of Yoda1 and PD150606 at 30 min. Representative microscopic fields after 3D reconstruction of phalloidin staining of T cells from each condition. (**E**) Area of surfaces generated from 3D reconstruction of phalloidin staining after application of the same-intensity threshold for each condition. (**F**) Colocalization of Piezo1 with the cortical actin scaffold was assessed by confocal microscopy in $CD4^+$ T cells in response to bead-immobilized anti-CD3/anti-CD28 Abs at 30 min. The *p* values were calculated using a Student *t* test. ns, not significant; NT, no treatment; PD150606>SOL +Yoda1, soluble anti-CD3/anti-CD28 Abs and Yoda1 following treatment with PD150606; SOL, soluble anti-CD3/anti-CD28 Abs.

synapse with the Ab-bearing beads (Fig. 4F). Thus Piezo1-driven Ca^{2+} influx links the mechanosensor to T cell activation through driving necessary cytoskeletal rearrangements for optimal TCR signaling, the mechanistic details of which warrant further studies.

Altogether, we have identified Piezo1 channels as a TCR-extrinsic mechanosensory module in human T cells (Fig. 5) that optimizes TCR activation. To our knowledge, this is the first report of the critical involvement of Piezo mechanosensors in the regulation of the immune response, and it opens up new avenues of research in the mechanoregulation of immune cells. Effective Piezo1 agonists can offer novel scalable methodologies for ex vivo expansion of T cells for anticancer immunotherapies, as well as the development of new-generation vaccine adjuvants, given the importance of optimal T cell activation in these contexts.

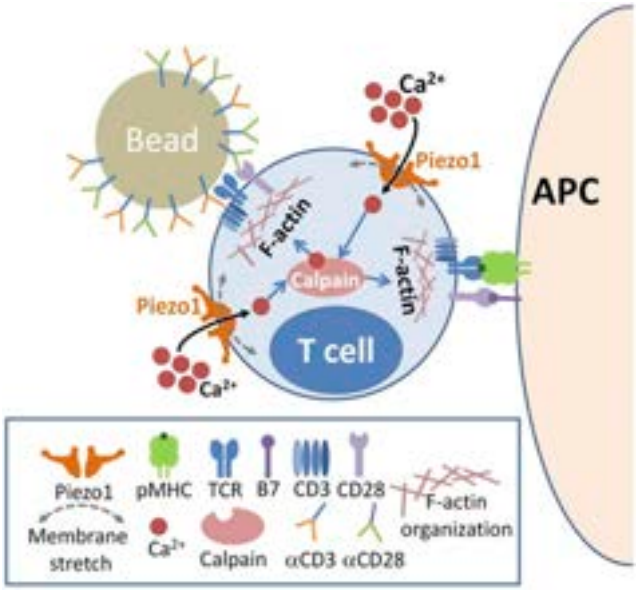

FIGURE 5. Proposed model for the role of Piezo1 in human T cell activation. Our data suggest that membrane stretch during immune synapse formation triggers Piezo1 activation and Ca^{2+} influx, which, in turn, activate calpain. Calpain activation helps in the organization of the cortical actin scaffold, thereby optimizing human T cell activation.

Acknowledgments

We acknowledge help from Suvendra Nath Bhattacharyya (Council of Scientific and Industrial Research–Indian Institute of Chemical Biology) for sharing reagents and help with confocal microscopy.

Disclosures

The authors have no financial conflicts of interest.

References

1. Morris, G. P., and P. M. Allen. 2012. How the TCR balances sensitivity and specificity for the recognition of self and pathogens. *Nat. Immunol.* 13: 121–128.
2. Malissen, B., and P. Bongrand. 2015. Early T cell activation: integrating biochemical, structural, and biophysical cues. *Annu. Rev. Immunol.* 33: 539–561.
3. Chen, W., and C. Zhu. 2013. Mechanical regulation of T-cell functions. *Immunol. Rev.* 256: 160–176.

4. Kim, S. T., K. Takeuchi, Z. Y. Sun, M. Touma, C. E. Castro, A. Fahmy, M. J. Lang, G. Wagner, and E. L. Reinherz. 2009. The alphabeta T cell receptor is an anisotropic mechanosensor. *J. Biol. Chem.* 284: 31028–31037.
5. Li, Y. C., B. M. Chen, P. C. Wu, T. L. Cheng, L. S. Kao, M. H. Tao, A. Lieber, and S. R. Roffler. 2010. Cutting edge: mechanical forces acting on T cells immobilized via the TCR complex can trigger TCR signaling. *J. Immunol.* 184: 5959–5963.
6. Coste, B., J. Mathur, M. Schmidt, T. J. Earley, S. Ranade, M. J. Petrus, A. E. Dubin, and A. Patapoutian. 2010. Piezo1 and Piezo2 are essential components of distinct mechanically activated cation channels. *Science* 330: 55–60.
7. Coste, B., B. Xiao, J. S. Santos, R. Syeda, J. Grandl, K. S. Spencer, S. E. Kim, M. Schmidt, J. Mathur, A. E. Dubin, et al. 2012. Piezo proteins are pore-forming subunits of mechanically activated channels. *Nature* 483: 176–181.
8. Pathak, M. M., J. L. Nourse, T. Tran, J. Hwe, J. Arulmoli, D. T. Le, E. Bernardis, L. A. Flanagan, and F. Tombola. 2014. Stretch-activated ion channel Piezo1 directs lineage choice in human neural stem cells. *Proc. Natl. Acad. Sci. USA* 111: 16148–16153.
9. Li, J., B. Hou, S. Tumova, K. Muraki, A. Bruns, M. J. Ludlow, A. Sedo, A. J. Hyman, L. McKeown, R. S. Young, et al. 2014. Piezo1 integration of vascular architecture with physiological force. *Nature* 515: 279–282.
10. Faucherre, A., K. Kissa, J. Nargeot, M. E. Mangoni, and C. Jopling. 2014. Piezo1 plays a role in erythrocyte volume homeostasis. *Haematologica* 99: 70–75.
11. Cahalan, S. M., V. Lukacs, S. S. Ranade, S. Chien, M. Bandell, and A. Patapoutian. 2015. Piezo1 links mechanical forces to red blood cell volume. *Elife* 4: e07370.
12. Wang, S., R. Chennupati, H. Kaur, A. Iring, N. Wettschureck, and S. Offermanns. 2016. Endothelial cation channel PIEZO1 controls blood pressure by mediating flow-induced ATP release. *J. Clin. Invest.* 126: 4527–4536.
13. Koser, D. E., A. J. Thompson, S. K. Foster, A. Dwivedy, E. K. Pillai, G. K. Sheridan, H. Svoboda, M. Viana, L. D. Costa, J. Guck, et al. 2016. Mechanosensing is critical for axon growth in the developing brain. *Nat. Neurosci.* 19: 1592–1598.
14. Woo, S. H., S. Ranade, A. D. Weyer, A. E. Dubin, Y. Baba, Z. Qiu, M. Petrus, T. Miyamoto, K. Reddy, E. A. Lumpkin, et al. 2014. Piezo2 is required for Merkel-cell mechanotransduction. *Nature* 509: 622–626.
15. Ranade, S. S., S. H. Woo, A. E. Dubin, R. A. Moshourab, C. Wetzel, M. Petrus, J. Mathur, V. Bégay, B. Coste, J. Mainquist, et al. 2014. Piezo2 is the major transducer of mechanical forces for touch sensation in mice. *Nature* 516: 121–125.
16. Syeda, R., J. Xu, A. E. Dubin, B. Coste, J. Mathur, T. Huynh, J. Matzen, J. Lao, D. C. Tully, I. H. Engels, et al. 2015. Chemical activation of the mechano-transduction channel Piezo1. *Elife* 4: e07369.
17. Wu, J., A. H. Lewis, and J. Grandl. 2017. Touch, tension, and transduction - the function and regulation of Piezo ion channels. *Trends Biochem. Sci.* 42: 57–71.
18. Lewis, R. S. 2001. Calcium signaling mechanisms in T lymphocytes. *Annu. Rev. Immunol.* 19: 497–521.
19. Schmidt, J. M., J. Zhang, H. S. Lee, M. H. Stromer, and R. M. Robson. 1999. Interaction of talin with actin: sensitive modulation of filament crosslinking activity. *Arch. Biochem. Biophys.* 366: 139–150.
20. Bate, N., A. R. Gingras, A. Bachir, R. Horwitz, F. Ye, B. Patel, B. T. Goult, and D. R. Critchley. 2012. Talin contains a C-terminal calpain2 cleavage site important in focal adhesion dynamics. *PLoS One* 7: e34461.
21. Selliah, N., W. H. Brooks, and T. L. Roszman. 1996. Proteolytic cleavage of alpha-actinin by calpain in T cells stimulated with anti-CD3 monoclonal antibody. *J. Immunol.* 156: 3215–3221.
22. Dustin, M. L., and D. Depoil. 2011. New insights into the T cell synapse from single molecule techniques. *Nat. Rev. Immunol.* 11: 672–684.
23. Comrie, W. A., and J. K. Burkhardt. 2016. Action and traction: cytoskeletal control of receptor triggering at the immunological synapse. *Front. Immunol.* 7: 68.